NASA TECHNICAL NOTE

NASA TN D-3036

NASA TN D-3036

COLLOID THRUSTOR BEAM ANALYSIS:

DESIGN AND OPERATION OF A SUITABLE QUADRUPOLE MASS FILTER

by Carl T. Norgren, Daniel S. Goldin, and Denis J. Connolly

Lewis Research Center
Cleveland, Ohio

NATIONAL AERONAUTICS AND SPACE ADMINISTRATION • WASHINGTON, D. C. • OCTOBER 1965

NASA TN D-3036

COLLOID THRUSTOR BEAM ANALYSIS: DESIGN AND OPERATION OF A SUITABLE QUADRUPOLE MASS FILTER

By Carl T. Norgren, Daniel S. Goldin, and Denis J. Connolly

Lewis Research Center
Cleveland, Ohio

NATIONAL AERONAUTICS AND SPACE ADMINISTRATION

For sale by the Clearinghouse for Federal Scientific and Technical Information
Springfield, Virginia 22151 – Price $2.00

COLLOID THRUSTOR BEAM ANALYSIS: DESIGN AND OPERATION OF A SUITABLE QUADRUPOLE MASS FILTER

by Carl T. Norgren, Daniel S. Goldin, and Denis J. Connolly

Lewis Research Center

SUMMARY

A quadrupole mass filter and a monopole spectrometer were designed and calibrated to be used in the analysis of the beam produced by a colloid thrustor. The mechanical and electrical design of the quadrupole mass filter is presented along with detailed calibration and test data. Only limited calibration data are presented for the monopole spectrometer because absolute transmission proved to be inadequate for the intended application.

The quadrupole mass filter was designed for a resolution of 10 (for particles accelerated through a 14 000-V potential), a constant radiofrequency voltage of 1000, and a variable-frequency mode of operation so that an atomic mass unit per unit electron charge range from 10 to 10^9 could be scanned. The quadrupole was calibrated with singly and doubly charged mercury ions accelerated through potentials from 500 to 48 000 volts.

It is shown that the beam mass-to-charge distribution can be determined within a maximum quadrupole design error of 7 percent. Use of the quadrupole mass filter to determine the average atomic mass unit per unit electron charge produced by a condensation-colloid thrustor is described, and comparison is made with previous colloid mass determinations obtained from photomicrographs and thrust-and-current measurements.

INTRODUCTION

One of the most important problems in evaluating the performance of a colloid thrustor is determination of the overall thrustor efficiency (ref. 1). Since the presence of molecular fragments or very heavy agglomerates in a charged colloid beam may lead to severe losses in thrustor efficiency, this determination requires an accurate knowledge

of the exhaust beam mass-to-charge spectrum, which under some extremes can include particles from 10 to 10^9 amu/z (atomic mass units per unit electron charge). The problems involved in such a measurement preclude the use of most conventional measuring techniques due to the high energy and the wide amu/z range of the particles in the colloid beam. In considering instruments to make such a measurement, the recently developed quadrupole mass filter and the similar monopole spectrometer appear worthy of investigation.

The basic theory of operation of the quadrupole (or monopole) mass filter and its application to the analysis of ionic beams are well documented for relatively low-energy low-molecular-weight ionic beams (refs. 2 to 6). Although the quadrupole mass filter has been used in the analysis of colloid beams (refs. 7 to 10), there is insufficient analytical or experimental data reported to show that these adaptations accurately measured the entire charged particle spectrum possible. If the quadrupole mass filter is to be used to measure quantitatively the exhaust spectrum produced by a colloid thrustor with the required range and accuracy, specialized techniques are necessary. These include operation in the variable-frequency mode, optimization of the applied voltage signals, precise control of voltage fluctuations, and proper choice of quadrupole probe dimensions to obtain a resolution compatible with experimental beam conditions. The required modifications and specialized techniques necessary to accomplish these goals and the results of these developments are described herein.

QUADRUPOLE DESIGN

A schematic diagram of the quadrupole mass filter is shown in figure 1(a). The basic operational characteristic is that of an amu/z filtering action. For a properly chosen setting of parameters (direct-current voltage U, radiofrequency voltage V, excitation frequency f, and field radius r_0) the quadrupole transmits only particles within a given amu/z band. (Symbols are defined in appendix A.) If it is assumed that the collector current represents the relative abundance of a given species, the quadrupole settings can be related to the quantitative amu/z spectrum of the colloid beam. Therefore, examination of the quadrupole theory is necessary to determine under what modes of operation and with what accuracy the preceding measurements are possible. A summary of the quadrupole theory as applied to this report is presented in appendix B.

A schematic diagram of the monopole spectrometer is shown in figure 1(b). The operational characteristics of the monopole spectrometer are similar to that of the quadrupole mass filter, in that for a similar set of operating parameters a given amu/z species will be collected. Theoretical advantages of the monopole spectrometer include simplified signal generator requirements and simplified mechanical construction com-

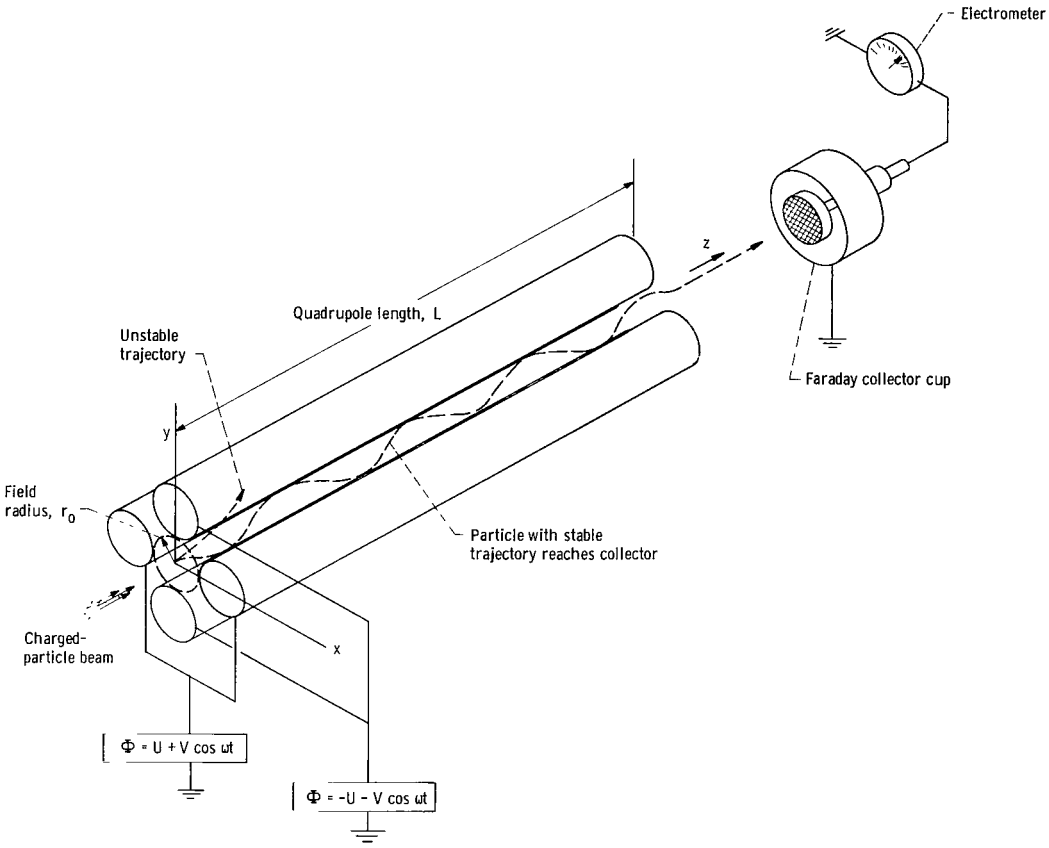

(a) Quadrupole mass filter.

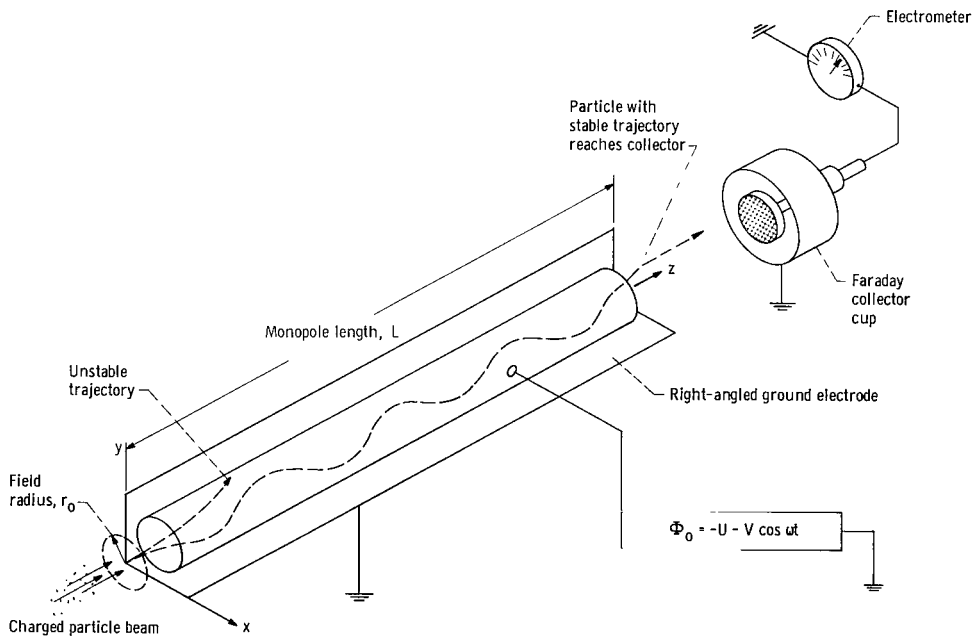

(b) Monopole spectrometer.

Figure 1. - Schematic diagram of mass analyzer.

pared with the quadrupole. However, the collected current intensity is expected to be somewhat less than that of the quadrupole due to impingement of stable trajectories on the angled ground electrode. A summary of the monopole spectrometer theory is also presented in appendix B.

Selection of Electrical and Mechanical Parameters

It is shown in reference 1 than an amu/z distribution in the exhaust beam of a colloid thrustor can be related to the overall colloid thrustor efficiency by an expression of the form (eq. (C4), appendix C)

$$\eta = \frac{1.043\times10^{-8}\, J_B}{\dot{m}_T\left(1 + \frac{P_\ell}{J_B\varphi}\right)} \langle \text{amu/z} \rangle\, \eta_d \tag{1}$$

Here $\langle \text{amu/z} \rangle$ is the average value determined from the amu/z spectrum, η_d is the distribution efficiency, and J_B, P_ℓ, and φ represent the thrustor parameters (beam current, total power losses, and accelerating potential, respectively).

The quadrupole mass filter was designed to produce an error of less than 7 percent in the determination of $\eta_d \langle \text{amu/z} \rangle$. As indicated in appendix C, this 7-percent permissible error in the determination of the exhaust spectrum can be distributed among the quadrupole operating parameters as follows:

(1) ϵ_1, 0.1 percent, error due to imperfect resolution (eq. (C5))

(2) ϵ_3, 1 percent, error in radiofrequency voltmeter reading

(3) ϵ_4, 1.5 percent, estimated error in field simulation

(4) ϵ_5, 0.5 percent, error in recording the frequency

(5) ϵ_6, 2 percent estimated error due to variation in collected current intensity

Details of error assignments and their interrelations (since the various values of ϵ do not sum directly) are given in appendix C.

As discussed in appendix B, the radiofrequency (rf) and direct-current (d-c) voltages, V and U, were fixed to establish the a/q operating slope (a/q = 2U/V), and the frequency was varied to provide the amu/z scan range of from 10 to 10^9. Equation (B15) can be rearranged to separate the quadrupole operating parameters from the colloid thrustor parameters:

$$\alpha \equiv \frac{L^2}{r_o^2}\frac{V}{R} = 170.5\,\varphi \tag{2}$$

All the fixed quadrupole parameters and the resolution R (which is defined as amu/z/Δamu/z have been included in the factor α, which is designated as the design difficulty factor and which is directly proportional to the colloid thrustor net accelerating potential φ. Substituting a value of 14 000 volts for the thrustor accelerating potential results in a value of $\alpha = 2.38\times10^{6}$. The larger the value of φ or α, the more difficult it will be to design the quadrupole. (Larger values of α require higher voltages, smaller rod sizes, and longer lengths, which complicate design considerations.)

In general, the design and fabrication of an rf signal generator is greatly simplified by avoiding high voltages. From equation (2), it is evident that the rf voltage is reduced by reducing r_o and increasing L. Reducing the resolution R would also help, but this parameter is limited to a value of at least 10 by the permissible error (appendix C). The limitations to be considered in determining a minimum r_o are the fabrication tolerance and rf voltage breakdown. Inherent in the 1.5-percent field-simulation error ϵ_4 is 1 percent contributed by using cylindrical rods rather than hyperbolic rods to produce the focusing field. This leaves 0.5 percent as an allowable fabrication variation, which when used with a fabrication tolerance of $\pm1\times10^{-5}$ meter results in a minimum radius r_o of 2×10^{-3} meter.

Before a breakdown criterion can be established for this rod spacing, it is necessary to determine the rf voltage that, in turn, depends on the length of the quadrupole. The quadrupole acts as an open-circuited transmission line and as such sets up standing waves that result in rf voltage variations along the rods, thus limiting the rod length. The voltage along the quadrupole rods can be given by (see ref. 11, e.g.)

$$V_L = V_o \cos\left(\frac{2\pi L}{\lambda}\right) \tag{3}$$

where V_o is the receiving end voltage, V_L is the applied voltage at the sending end, L is the axial distance along the quadrupole rod from the receiving end, and λ is the free-space wavelength of the signal. If the length of the rod is less than $\lambda/4$, the minimum voltage will be at the sending end. The voltage variation along the length of the quadrupole is given by

$$\frac{V_o - V_L}{V_o} = 1 - \cos\frac{2\pi L}{\lambda}$$

or, with $\lambda = c/f$,

$$L = \frac{c}{2\pi f}\cos^{-1}\left(1 - \frac{V_o - V_L}{V_o}\right) \tag{4}$$

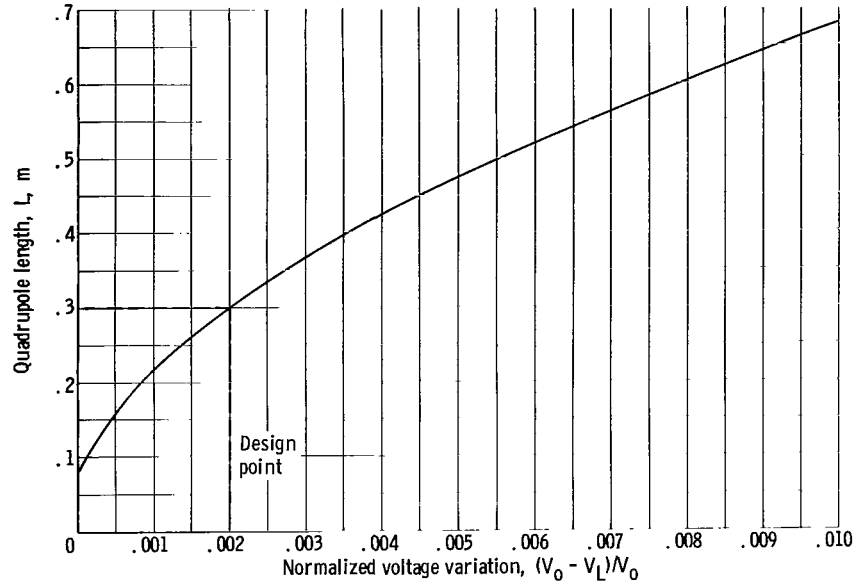

Figure 2. - Quadrupole length for normalized voltage variation along rods. Frequency, 10 megacycles.

Shown in figure 2 is a plot of quadrupole length as a function of $(V_0 - V_L)/V_0$ for a frequency of 10 megacycles. The upper limit of 10 megacycles was chosen from practical considerations to avoid excessive power requirements. Previously the maximum error in the voltmeter reading of V was specified to be 1 percent (appendix C). Choosing $(V_0 - V_L)/V_0 \approx 1/5\ \epsilon_3$ makes the voltage variation along the length of the rod small in comparison with the total voltage error. Therefore, from figure 2, if $(V_0 - V_L)/V_0 = 0.002$, the maximum quadrupole length should be 0.30 meter. The values of r_0 2×10^{-3} meter, L = 0.3 meter, R = 10, and $\alpha = 2.387\times10^6$ can now be substituted into equation (2) to yield V = 1052 volts. Radiofrequency voltage breakdown criteria for $r_0 = 2\times10^{-3}$ meter (ref. 12) indicate that it would be possible to support a voltage an order of magnitude greater than V and still avoid breakdown.

The frequency range necessary to scan for colloids in the range from 10 to 10^9 amu/z, obtained by equation (B7a) and the values of V and r_0, as determined previously, is from 1.93 kilocycles to 19.3 megacycles. This upper frequency of 19.3 megacycles (corresponding to 10 amu/z) is greater than the selected frequency limit of 10 megacycles, which corresponds to an amu/z of 36.4 (for V = 1052 V, r_0 = 2 mm, and R = 10). The range from 36.4 to 10 amu/z, however, can be reached with the frequency limited to 10 megacycles by scanning with a lowered rf voltage. The reduction in rf voltage is reflected in a decreased resolution that results in an increase in the distribution error ϵ_1 to 0.4 percent (see appendix C). This additional error will not significantly increase the maximum design error of 7 percent and is therefore acceptable for the small portion of the amu/z range involved.

The quadrupole operating slope a/q can be expressed in terms of U and V from equations (B6b) and (B7b) as

$$\frac{a}{q} = \frac{2U}{V} \tag{5}$$

Equation (B12) can be used to express the d-c voltage in terms of R and V as

$$U = \frac{V(0.1678\,R - 0.126)}{R} \tag{6}$$

Using V = 1052 volts and R = 10 results in a d-c voltage of 163 volts and an a/q operating slope (2U/V) of 0.310. The quadrupole specifications are summarized as follows:

Error in determining $\eta_d \langle amu/z \rangle$, percent	±7
Scan range, amu/z	10 to 10^9
Frequency range, kc to Mc	1.93 to 10
Resolution, R	10
Field radius (see fig. 1(a)), r_o, m	$2\times10^{-3} \pm 1\times10^{-5}$
Field length, L, m	3×10^{-1}
rf Voltage (±1 percent), V, V	1052
d-c Voltage, U, V	163

SIGNAL GENERATORS

The signal required for the quadrupole mass filter consists of d-c and rf voltages impressed on opposite pairs of equally spaced cylindrical rods (see fig. 1(a)). The rf component of the required signal consists of two constant-amplitude sinusoidal voltages each 1052 volts peak with a mutual phase angle of 180°. In practice, the design value of the rf voltage was rounded off to 1000 volts to provide additional control voltage. The frequency of the rf signal must be continuously variable from about 2.0 kilocycles to 10 megacycles. To accomplish this, both low- and high-frequency signal generators were used. In addition, separate sources were required for the positive and negative d-c voltage signals. The constancy of the ratio 2U/V depended only on commercially available rf voltmeter probes as detectors for the automatic level control. The output of the rf voltage signal generators was capacitively coupled to the terminals of the quadrupole, and the appropriate d-c voltages were superimposed. Complete commercial rf signal generators capable of producing rf voltage of the required constancy

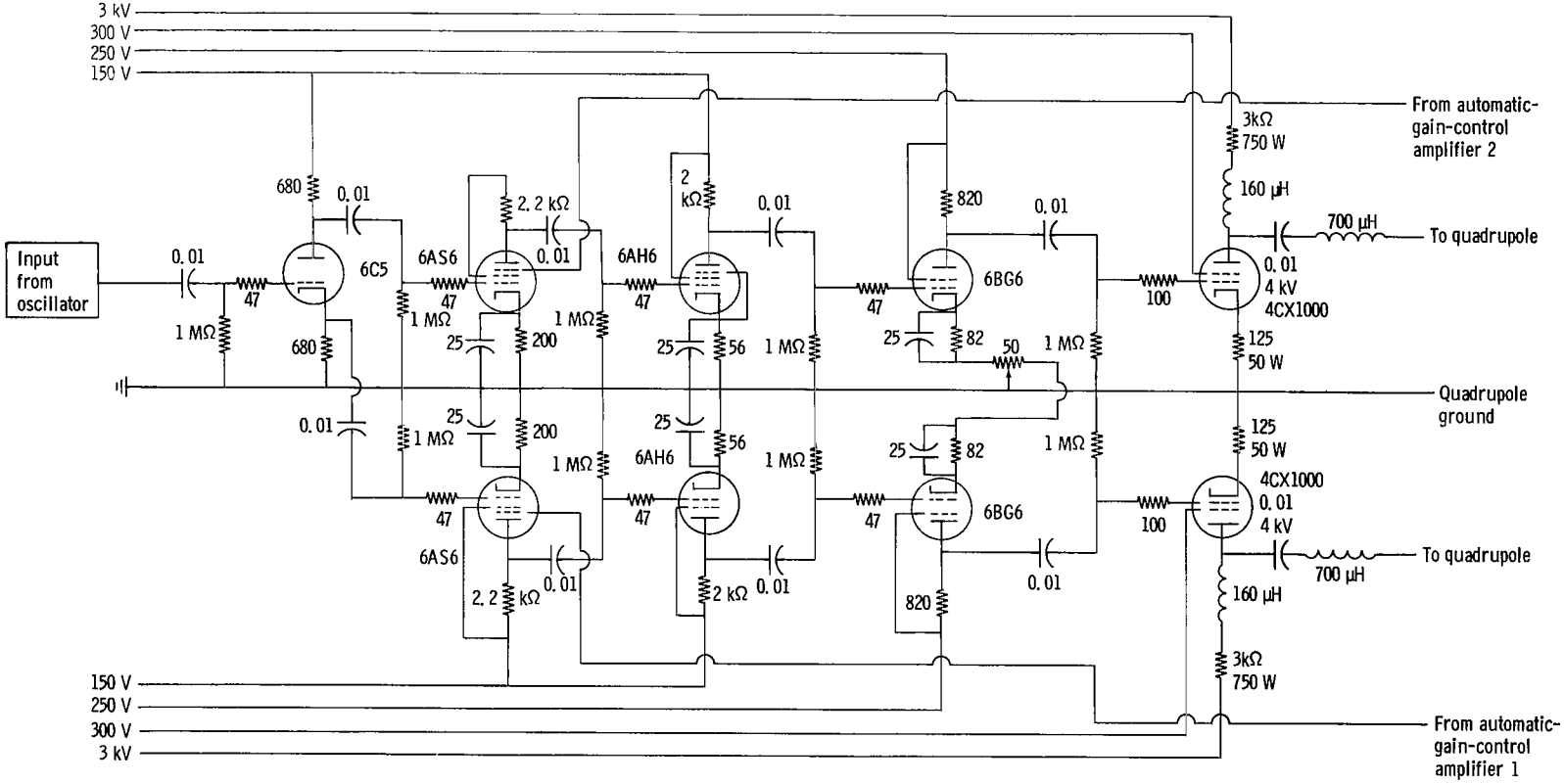

Figure 3. - Schematic diagram of low-frequency (1 kC to 0.500 Mc) signal generator. (All resistors are in ohms, and all capacitors are in microfarads unless otherwise noted.)

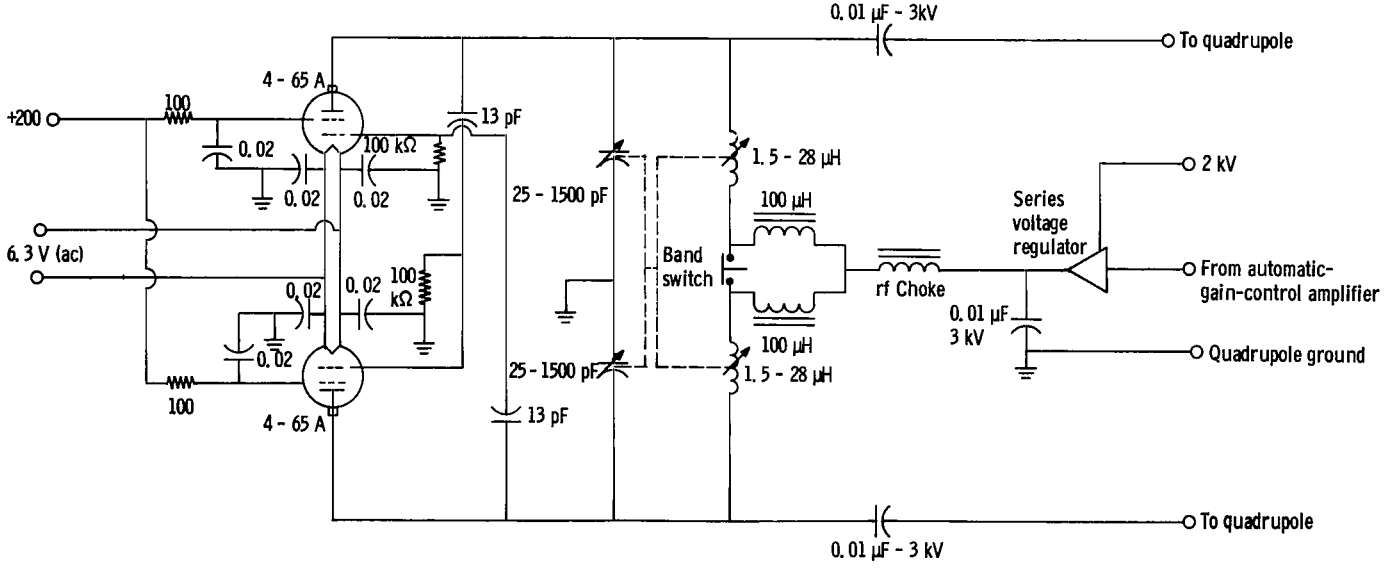

Figure 4. - Schematic diagram of high frequency (0.500 to 10 Mc) signal generator. (All resistors are in ohms and all capacitors in microfarads unless otherwise noted.)

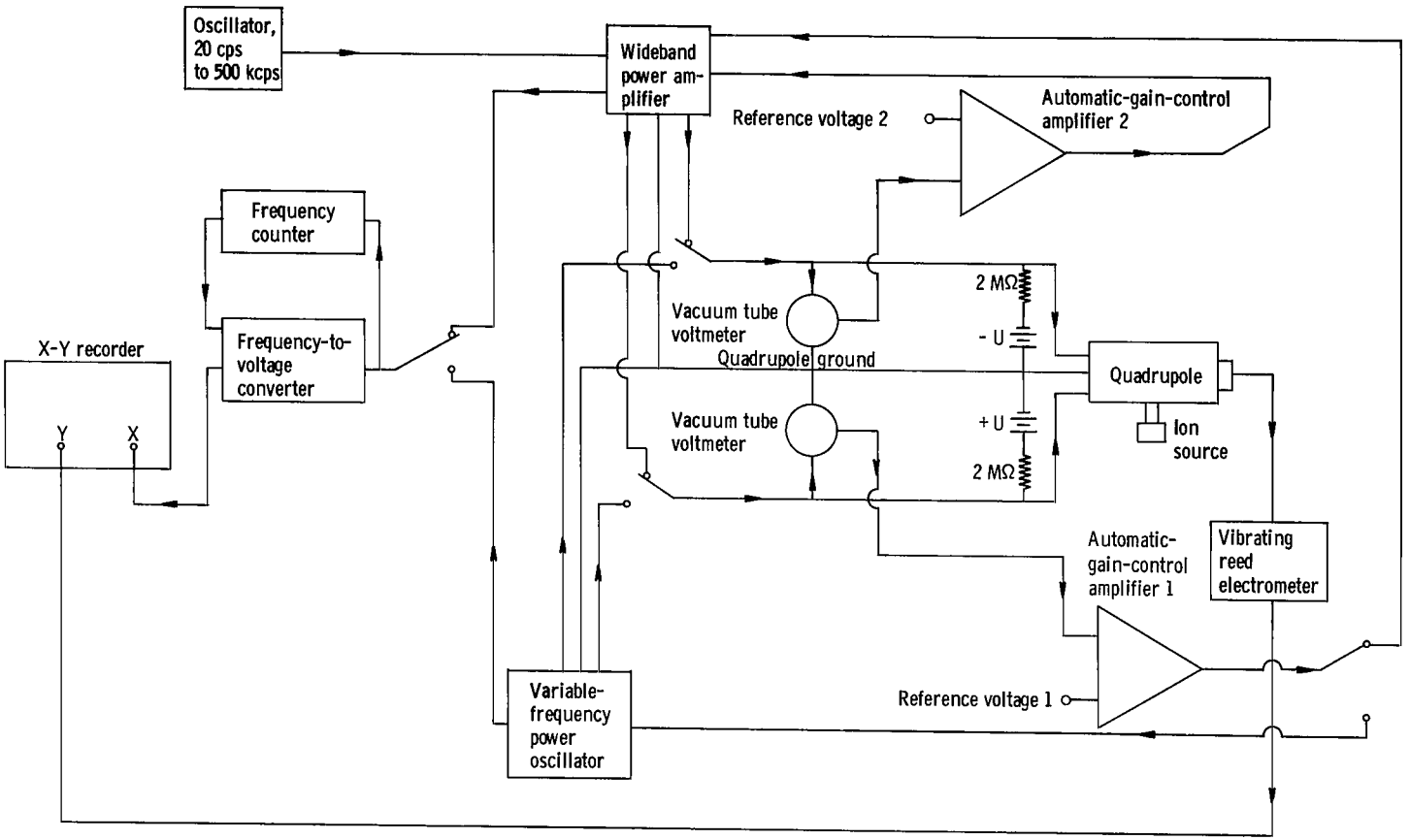

Figure 5. - Readout equipment for experimental quadrupole mass filler system.

and magnitude were not available. Consequently, those components that were built by in-house projects are described in detail.

Low-Frequency Signal Generator

The method of generating the signal in the range from 2.0 kilocycles to 0.5 megacycle that was developed is shown schematically in figure 3. A commercially available oscillator (not shown) was used to drive a 6C5 phase splitter, the two outputs of which were equal and 180^{o} out of phase. Each of these outputs fed the input of a wide-band amplifier; the first stage has voltage variable gain, and the last stage is capable of supplying the required voltage to the capacitive load of the quadrupole. In order to provide automatic level control, the output of each rf voltmeter was compared with a reference voltage, and the difference was amplified and fed back to the control electrode of the appropriate input stage. Thus, the output voltage of each channel was constrained to remain constant during a frequency scan, the error being only that due to the variation in properties of the rf voltmeter probe. Probe signal variation was within ±0.2 percent over the frequency range of interest.

High-Frequency Signal Generator

The method of generating the signals in the range from 0.5 to 10 megacycles that was developed is shown schematically in figure 4. The signal was generated at the required level by a balanced push-pull oscillator configuration. The two vacuum-variable capacitors were carefully balanced, and the electrical center of the two inductors was allowed to float by feeding the plate supply voltage through a choke coil. Thus, the two output voltages were constrained to have adequate amplitude and phase balance without independent control. To achieve automatic level control, it was merely necessary to use either amplified error voltage to drive a series regulator in the plate supply line.

Readout Equipment

The entire quadrupole system is shown schematically in figure 5. The readout equipment included an electronic counter, a vibrating-reed electrometer, two rf vacuum-tube voltmeters, a digital voltmeter, a frequency-to-analog converter, and an X-Y recorder. The frequency-to-analog converter provided a d-c signal proportional to the frequency used to drive the x-axis of the recorder. The counter was used to

monitor the frequency and to calibrate the X-Y recorder. The y-axis of the recorder was driven by the output of the vibrating-reed electrometer. The vacuum-tube voltmeters monitored each rf voltage, and the analog outputs provided voltages proportional to the rf input and independent of frequency to within less than ±0.2 percent.

TEST APPARATUS

Electron-Bombardment Thrustors

A 10-centimeter-diameter electron-bombardment thrustor was used as the calibration ion source from 500 to 6000 volts (fig. 6). This ion source was similar to that previously reported in reference 13; however, no magnetic field was used, and an electrically heated vaporizer was substituted for the steam boiler. A 20-centimeter-diameter electron-bombardment thrustor was used as the calibration ion source from 12 000 to 48 000 volts (fig. 7). In both thrustors, propellant flows through an orifice between the vaporizer and the flow distributor. After leaving the distributor it enters the ion chamber. Electrons from a hot filament on the axis of the ion chamber bombard the neutral atoms and create a plasma. The ions created pass through the screen and out the accelerator.

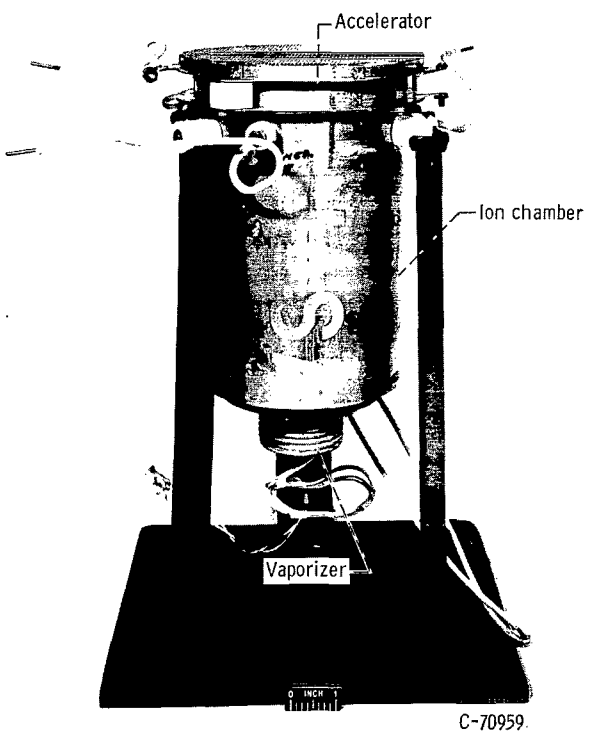

Figure 6. - Low voltage (500 to 6000V) 10-centimeter-diameter electron-bombardment thrustor.

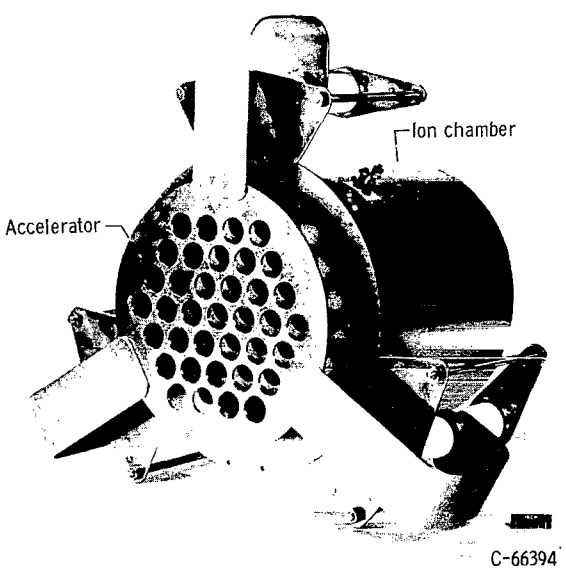

Figure 7. - High-voltage (12 000 to 48 000) 20-centimeter-diameter electron-bombardment thrustor.

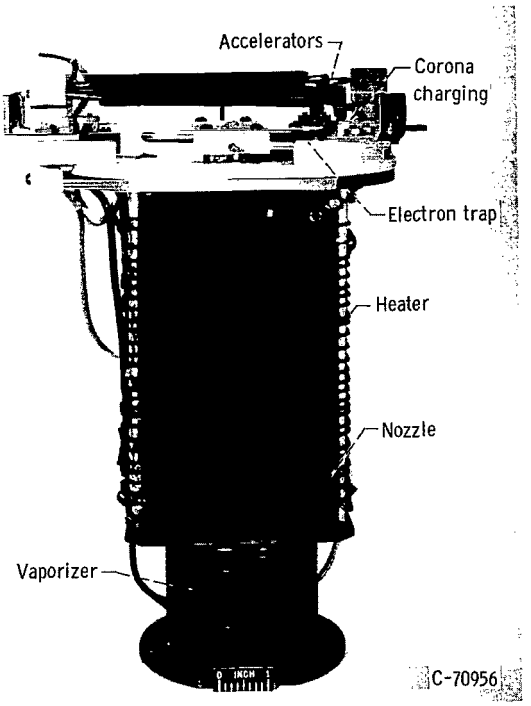

(a) Colloid thrustor.

Figure 8. - Experimental condensation colloid thrustor.

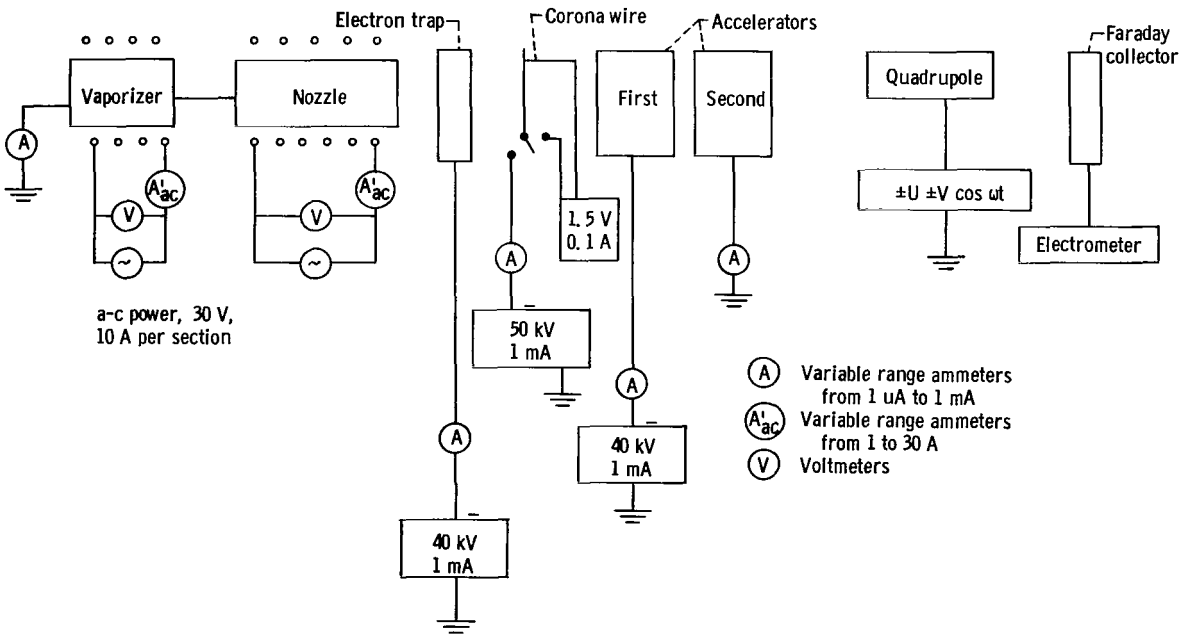

(b) Power supply and metering system.

Figure 8. - Concluded. Experimental condensation colloid thrustor.

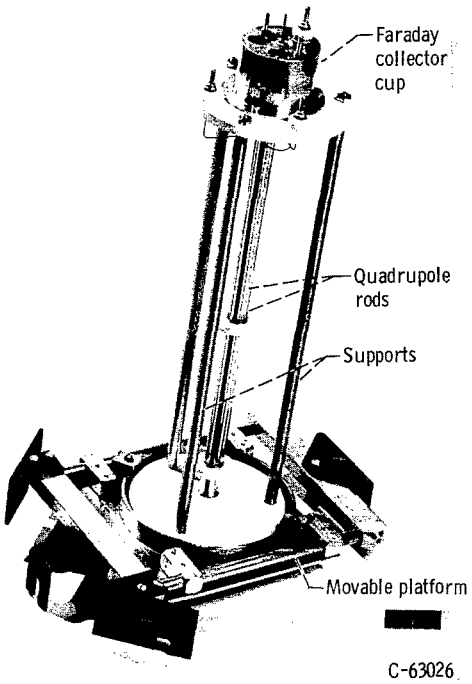

Figure 9. - Experimental quadrupole mass filter.

Colloid Thrustor

A colloid thrustor (refs. 14 and 15) shown in figure 8(a) provided the charged particle beam for the experimental investigation. In operation, a vaporized propellant is rapidly cooled by an adiabatic expansion through a convergent-divergent nozzle until a condensation shock occurs. The stable nuclei formed in the condensation shock region continue through a relatively slow growth phase and are subsequently negatively charged by a corona discharge. The charged colloids are then accelerated from the corona potential to ground by Pierce accelerators. A schematic diagram of the experimental arrangement is shown in figure 8(b).

The propellant stagnation temperature was controlled by varying the power input to the electrically heated vaporizer. The convergent-divergent nozzle was heated to prevent condensation on the walls.

Mass Filters

The quadrupole mass filter is shown in figure 9. The entire unit was encased in a copper shield. A shielded Faraday cup with a titanium honeycomb collector was used to meter collector current. The Faraday cup was connected by a shielded low-noise cable to the input of the electrometer. A 300-gauss magnetic field was used to suppress secondary electrons from the Faraday cup for inlet energies in excess of 20 000 volts. In tests with either the 10-centimeter-diameter electron-bombardment thrustor or the colloid thrustor, the quadrupole was positioned 0.02 meter from the thrustor exit. The tests with the 20-centimeter-diameter electron-bombardment thrustor were conducted in another, larger test facility, and it was necessary to locate the quadrupole about 3 meters from the thrustor in order to minimize lead lengths.

The inlet aperture was varied to determine its effect on the mercury collected current intensity. It has been shown experimentally, for cases where the particle accelerating voltage was less than that of the quadrupole rf voltage, that the optimum inlet aperture diameter should be a function of the reciprocal of the square root of the

resolution (i.e., orifice diameter $\approx r_o/\sqrt{R}$, ref. 2). This empirically determined aperture size is based on the minimum number of oscillations required to stabilize a particle to obtain 100-percent transmission.

In this application, three inlet apertures (0.3, 0.52, and 2.0 mm radius) were selected. The 0.3 millimeter inlet aperture ($\ell/D = 1$) represents the optimum entrance aperture where the accelerating voltage is less than the rf voltage. Since in this application the accelerating voltage could exceed the rf voltage the two additional apertures were included. The 0.52-millimeter aperture ($\ell/D = 10$) was used to determine the effect of physically columnating the inlet beam (e.g., removal of particles with a large transverse velocity component) as well as the effect of increased aperture size. The 2.0-millimeter aperture ($\ell/D = 1$) represents the extreme case of an inlet aperture equal to the quadrupole field radius (r_o).

The monopole spectrometer design was similar to that used for the quadrupole. The length was 0.30 meter, and the quadrupole field radius was 2 millimeters. Several inlet apertures were tested.

PROCEDURE

The following procedure was used for quadrupole or monopole operation. The system was installed in the vacuum facility, and the quadrupole rf and d-c signal generators and readout equipment were allowed to stabilize. All metering instruments were then checked against known standards, and rf phase relation and wave shapes were observed. The quadrupole was positioned on its movable platform to accept the maximum beam current.

The 10-centimeter-diameter electron-bombardment thrustor was operated with three propellants: mercury, stannic iodide, and mercurous chloride. A porous-plug-flow orifice was used for mercury operation; whereas, a 1.52-millimeter choked-flow orifice was used for the other propellants. Propellant flow was established, and thrustor potentials were applied. An ion-chamber potential of 110 volts and a constant beam current of 12 microamperes were maintained for values of thrustor accelerating potential of 500, 2000, 4000, and 6000 volts. The 10-centimeter-diameter thrustor was not operated at higher potentials because of electric breakdown limitations. The accelerating potentials of 12 000, 24 000, and 48 000 volts were obtained with the 20-centimeter-diameter electron-bombardment thrustor (fig. 7). During these tests, the quadrupole d-c to rf voltage ratio 2U/V was varied stepwise from 0 to 0.350 (at a constant V = 1000 V) to provide a wide range of operating slopes. Also, the rf voltage was varied stepwise from 250 to 1000 volts at a constant 2U/V of 0.310.

The colloid thrustor was operated with mercurous chloride as a propellant so that comparison could be made with previously obtained exhaust spectra as determined from photomicrographs and thrust-and-current measurements (refs. 14 and 15). The colloid thrustor was loaded with up to 50 grams of propellant. The thrustor potentials were established, and the vaporizer was brought to a predetermined stagnation temperature. The accelerating voltage was adjusted so that a stable corona current of approximately 6 microamperes was maintained. During colloid operation scans were performed with V = 1000 volts and the ratio 2U/V equal to 0.310. The continuous frequency variation from 1.93 kilocycles to 0.5 megacycle was obtained with the low-frequency generator. The frequency variation from 0.5 to 10 megacycles was accomplished by consecutive scanning of two ranges with the high-frequency generator: 0.5 to 1.5 megacycles, and 1.5 to 10 megacycles.

Calculations

The data reported herein were taken with the rf voltmeter leads connected to the quadrupole input leads external to the vacuum chamber. It was later found that the lead impedance from the connection to the actual quadrupole rods was not negligible at the upper end of the frequency range; consequently, the voltage actually applied to the quadrupole rods was different from that indicated by the voltmeter. This voltage error results in an error in the measured amu/z and a variation in the operating slope 2U/V over a given amu/z sweep. To correct the data for this effect, rf voltmeter readings as a function of frequency were taken with the voltmeter probes directly connected to the quadrupole rods. The resulting correction factor is shown in figure 10 as the ratio of actual to indicated rf voltage and was applied to all quadrupole data.

The following procedure was used to evaluate the experimental amu/z traces. Two representative scans are shown in figure 11. Intensities f_1 and f_2 are determined at the intersections corresponding to half-peak collected current. As discussed in appendix B, these frequencies can be related by equation (B7b) to obtain the values of $(amu/z)_1$ and $(amu/z)_2$. As shown in figure 11, the amu/z scan is trapezoidal with the low frequency side having a greater slope than the high-frequency side. This would be expected from a comparison with the stability plot described in appendix B (fig. 21). The experimental amu/z identified with each scan was obtained by the following relation:

$$amu/z \approx \left\{(amu/z)_2 - 0.17\left[(amu/z)_2 - (amu/z)_1\right]\right\} \tag{7}$$

This approximate expression relates the values of $(amu/z)_1$ and $(amu/z)_2$ to the experi-

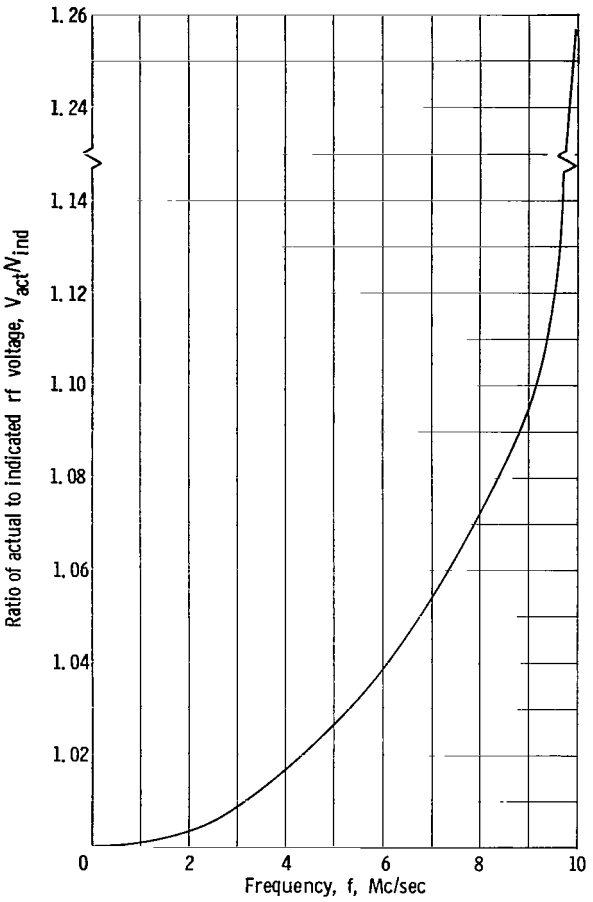

Figure 10. - Correction factor to determine actual rf voltage applied to quadrupole rods.

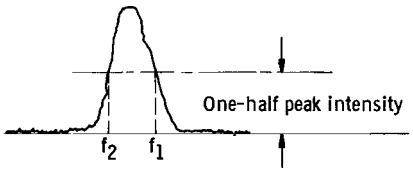

(a) Net accelerating potential, 2000 volts; resolution 11.3.

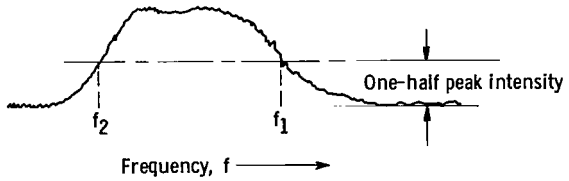

(b) Net accelerating potential, 48 000 volts; resolution, 5.4.

Figure 11. - Typical experimental singly charged mercury ion trace for two values of inlet particle energy at constant quadrupole operating slope of 0.313.

mental amu/z and is obtained by identifying the respective amu/z values with corresponding q values. (The factor 0.17 is equal to $(q_1 - q)/(q_1 - q_2)$, where $q = 0.706$.)

The experimental resolution was determined by using the amu/z value from equation (7) in the following expression:

$$R_{exp} = \frac{amu/z}{(amu/z)_2 - (amu/z)_1} \qquad (8)$$

RESULTS AND DISCUSSION

Quadrupole Mass Filter Calibration

Calibration was obtained primarily with singly and doubly charged mercury ions. Parameters considered include amu/z, transmission, and resolution as a function of the operating slope a/q, particle energy, and quadrupole rf voltage level for the 2-millimeter-inlet aperture size The effect of the 0.3- and 0.52-millimeter apertures on collected current is also presented in the transmission section.

Amu/z determinations. - The effects of a/q, inlet beam energy, and quadrupole rf voltage on the amu/z (determined from eq. (7)) for singly charged mercury ions are shown in figures 12(a) to (c), respectively. The effects of a/q on the amu/z for doubly charged mercury ions is shown in figure 13. The deviation of the singly charged mercury ions (200.6 amu/z) peak determined from the data of figure 12(a) is from -1.0 to -5.0 percent. The deviation for doubly charged mercury ions (100.3 amu/z) is from 0.8 to 2.8 percent. It is

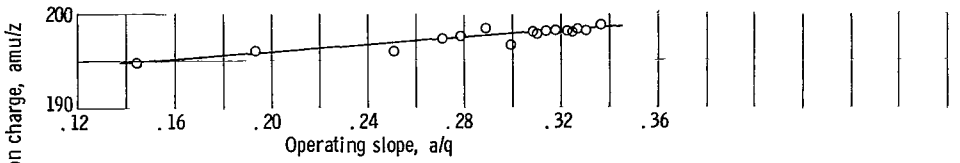

(a) Effect of operating slope. Net accelerating potential, 2000 volts; applied rf voltage, 1000 volts.

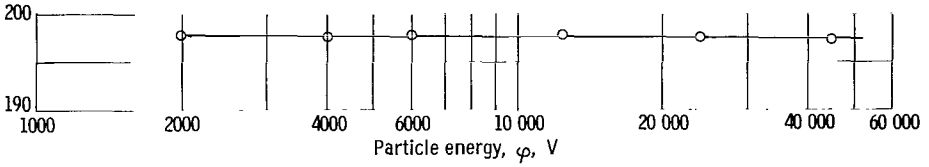

(b) Effect of particle energy. Operating slope, 0.310; applied rf voltage, 1000 volts.

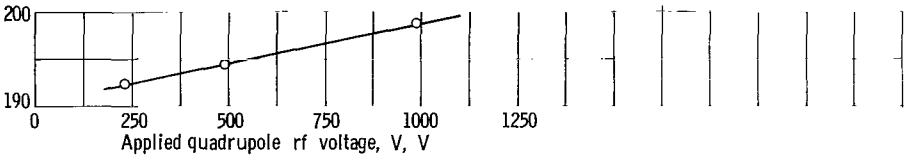

(c) Effect of rf voltage. Operating slope, 0.310; net accelerating potential, 2000 volts.

Figure 12. - Variation of experimental amu/z of singly charged mercury ions for three operating parameters. Ion chamber potential, 110 volts; total thrustor beam current, 12×10^{-6} ampere.

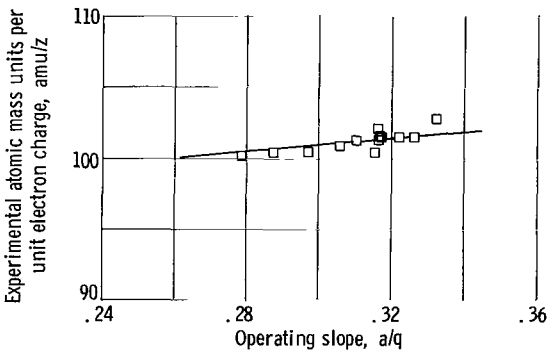

Figure 13. - Variation of experimental atomic mass units of doubly charged mercury ions for variation of operating slope. Ion chamber potential, 110 volts; total thrustor beam current, 12×10^{-6} ampere; net accelerating potential, 2000 volts; applied rf voltage, 1000 volts.

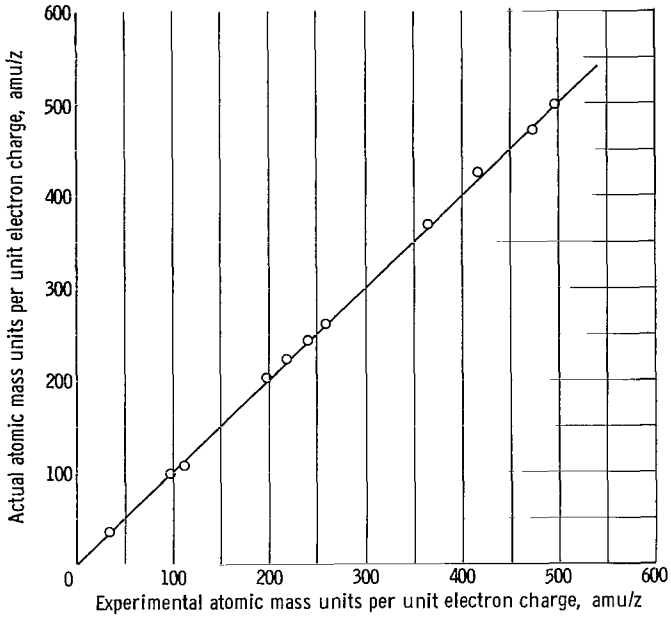

Figure 14. - Calibration of quadrupole mass filter for numerous ionic species. Total thrustor beam current, 12×10^{-6} ampere; net accelerating potential, 2000 volts; applied rf voltage, 1000 volts.

not known why the deviation was negative for singly charged mercury ions and positive for doubly charged mercury ions. In both cases, however, the deviation is within the allowable design error. In general, a/q and particle energy variations did not appreciably affect the amu/z (figs. 12(a) and (b)). There was about a 3-percent degradation in amu/z, however, as the rf voltage was decreased from 1000 to 250 volts at a constant a/q of 0.310 (equivalent to design resolution of 10), as shown in figure 12(c).

A comparison of theoretical and experimentally determined amu/z is shown in figure 14. These data were obtained with mercury, stannic iodide, and mercurous chloride in the electron-bombardment thrustor for a net accelerating potential of 2000 volts. The values of amu/z correspond to singly and doubly charged mercury ions (amu/z, 200.6 and 100.3, respectively) and to molecular fragments such as ionic stannic iodide (amu/z, 489.5). Simple molecular structures were investigated so that interpretation of complex fragmentation could be avoided and only major peak intensities considered.

Deviation of experimental values with respect to theoretical values is probably a result of the compromise in the selection of quadrupole parameters and inherent errors in readout equipment. Of all the species examined, the maximum deviation was -2.5 percent at the design resolution of 10. This accuracy is considered sufficient for meaningful thrust measurements in colloid thrustors. It is assumed that the established quadrupole focusing field is equally as effective in stabilizing colloidal particles ($amu/z \gg 500$) as in stabilizing ionic species ($amu/z < 500$).

Mercury-collected current intensity measurements. - The variation of collected current with quadrupole operating slope is shown in figures 15(a) and (b) for entering particle energies of 500 and 2000 electron volts, respectively, for the three different inlet aperture sizes and a constant quadrupole operating rf voltage of 1000 volts. For the 500-electron-volt particles (fig. 15(a)), collected current is constant for values of a/q up to approximately 0.310. For even lower energies (much less than the applied rf voltages) the expected limit is about 0.330 (refs. 2 to 5). It was not possible to operate the thrustor at such low voltages; however, if the inlet particle energy were

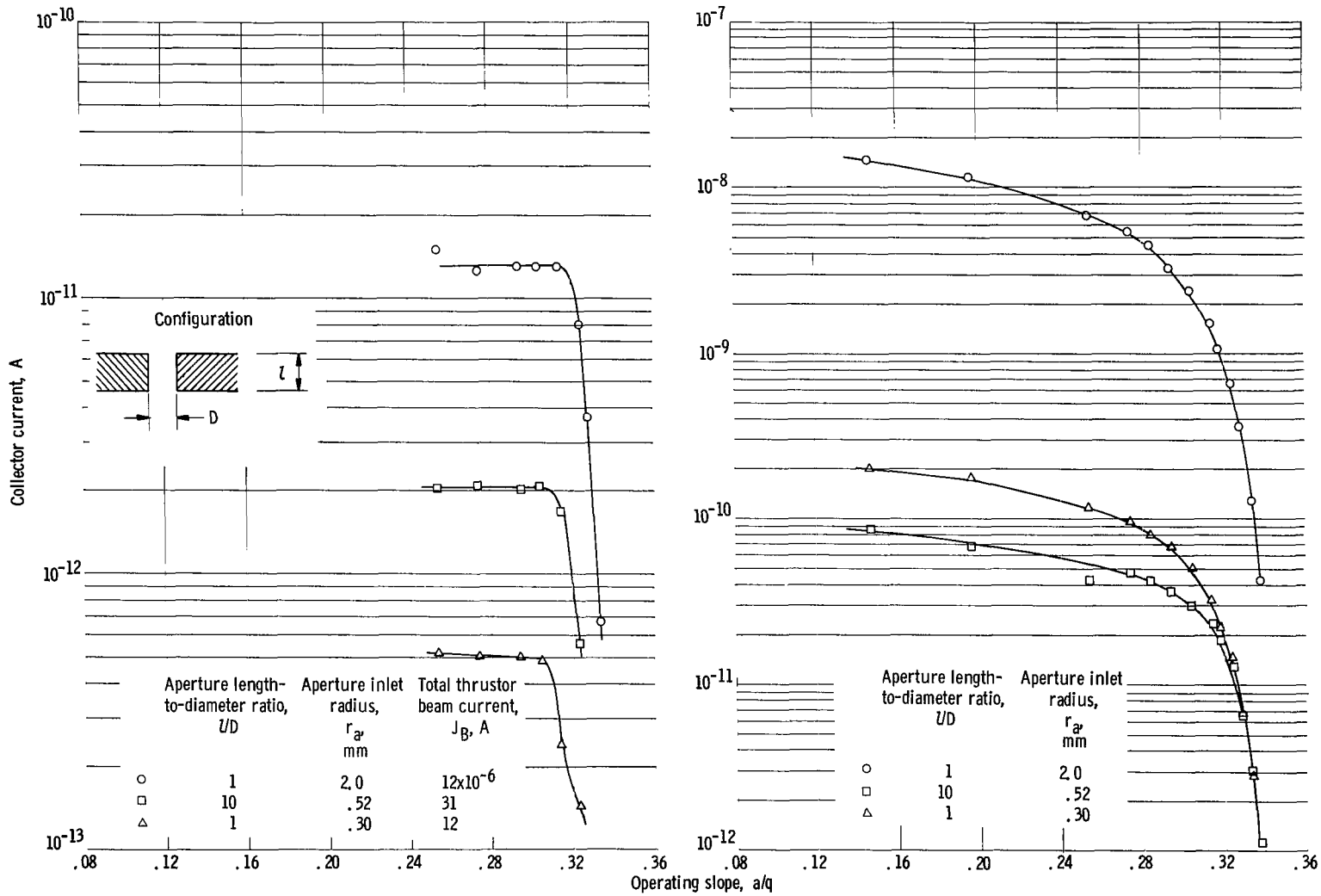

(a) Particle energy, 500 volts.

(b) Particle energy, 2000 volts; total thrustor beam current, 12×10^{-6} ampere.

Figure 15. - Collected current intensity for three aperture sizes. Ion chamber potential, 110 volts; applied rf voltage, 1000 volts.

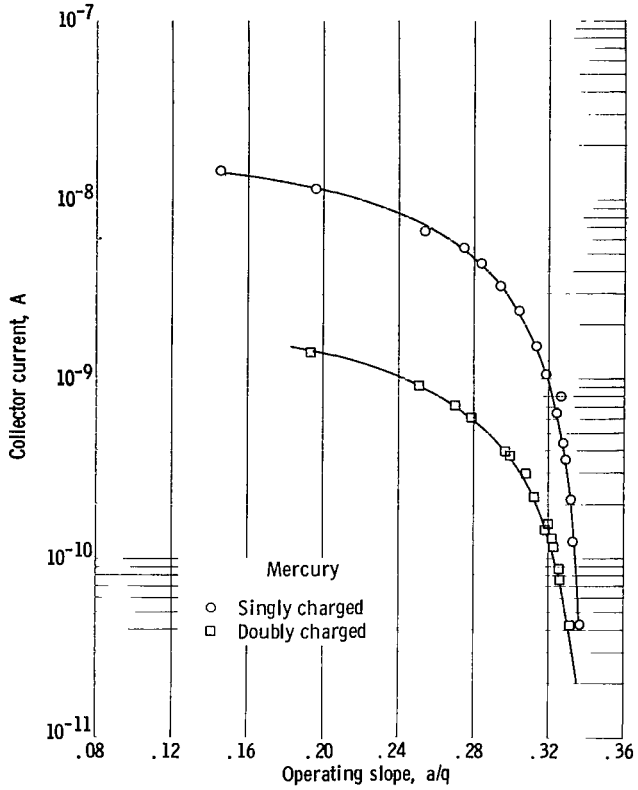

(a) Effect of operating slope. Net accelerating potential, 2000 volts; applied rf voltage, 1000 volts.

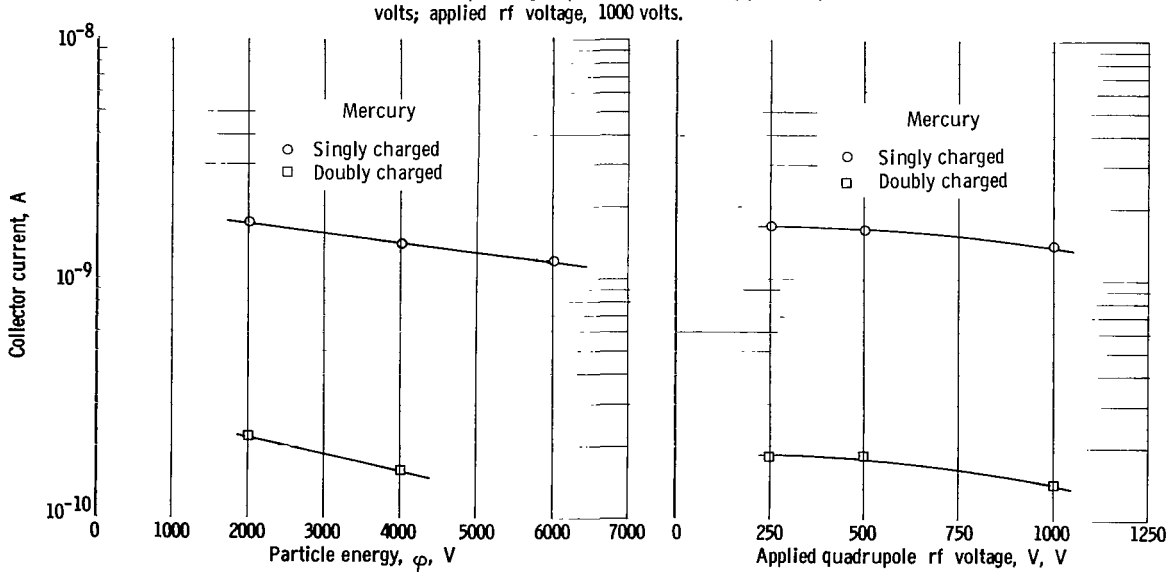

(b) Effect of particle energy. Operating slope, 0.310; applied rf voltage, 1000 volts.

(c) Effect of rf voltage. Operating slope, 0.310; net accelerating potential, 2000 volts.

Figure 16. - Variation of collected current of singly and doubly charged mercury. Ion chamber potential, 110 volts; total thrustor beam current, 12×10^{-6} ampere.

further reduced, this expected limit of 0.330 for the flat portion might be reached. For the 2000-electron-volt particles (fig. 15(b)), there is a complete absence of a constant-collected-current region for any aperture size tested. As the accelerating voltage was further increased (not shown in fig. 15) the slopes of the curves for collected current were similar. Since most of the previously reported data in the literature was in a regime where the quadrupole voltage was much greater than the accelerating voltage of the ions analyzed, the phenomenon of continuously variable transmission for all a/q values was not encountered. A possible explanation of the continuous variation in figure 15(b) is that, as the accelerating voltage was increased, the magnitude of the transverse component of the velocity also increased as a result of source ion optics and beam spread due to space charge. Quadrupole theory indicates that such an increase in value of transverse particle energy at the quadrupole inlet will reduce the transmission (ref. 2).

Comparing collected current variations for the various apertures (2.0, 0.52, and 0.3 mm radius) and for the estimated ±0.2-percent variation in rf probe voltage yields a possible variation in collected current intensity ϵ_6 of ±3.1, ±2.2, and ±3.1 percent, respectively. Thus, since none of the apertures offered a clear advantage in terms of minimum collected-current variation, the 2-millimeter aperture was chosen for operation. It permitted a level of collected current two orders of magnitude greater than the 0.52- and 0.3-millimeter apertures, thus greatly increasing quadrupole sensitivity. The error in ϵ_6 is greater than that selected (appendix C); however, applying the measured value of ϵ_6 with the measured values of $\epsilon_2 = 0.025$ and $\epsilon_1 = 0.001$ to equation (C9) results in an overall error in the quadrupole measurement of 5.6 percent, which is still below the desired maximum of 7 percent.

The collected intensity from the low-voltage ion source of singly and doubly charged mercury ions is shown in figures 16(a) to (c) for variation in a/q, inlet particle energy, and quadrupole rf voltage, respectively, for a 2-millimeter aperture. As shown in figure 16(b), a slight decrease in collector current was obtained as particle energy increased at the design operating slope of 0.310. This appears contradictory to the data of figure 15 (taken at lower accelerating voltages); however it is readily accounted for as a phenonemon associated with thrustor operating characteristics. In effect, with the beam current held constant, variations in accelerating voltage alter the ion optic characteristics of the thrustor (ref. 16). As indicated in figure 16(c), the quadrupole rf voltage level did not appreciably affect the ratio of the collected current of singly or doubly charged mercury ions over the voltage range investigated.

In figure 17 the relative intensities of singly and doubly charged mercury ions are plotted for a series of a/q ratios at an rf voltage of 1000 (from fig. 16(a)). The proportion of singly to doubly charged mercury ions is approximately 0.89, as determined by the quadrupole mass filter. A previous investigation (ref. 17) that used a permanent-

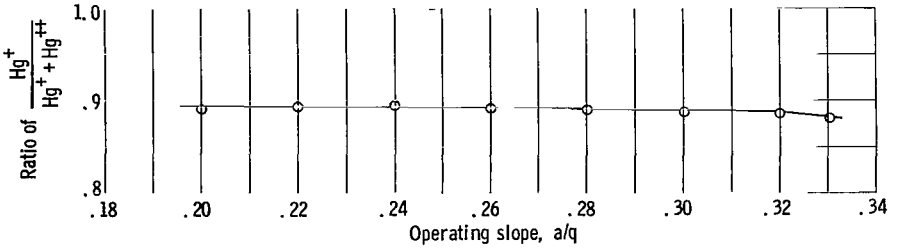

Figure 17. - Relative abundance of singly charged mercury ions in mixed beam containing singly and doubly charged mercury ions. Ion chamber potential, 110 volts; total thrustor beam current, 12×10^{-6} ampere; net accelerating potential, 2000 volts; applied rf voltage, 1000 volts.

magnet-type mass spectrometer reported a ratio of approximately 0.86 in a beam obtained under comparable operating conditions. This close agreement of about 3 percent indicates that the quadrupole is capable of determining the relative abundance of a beam of multiple species with a reasonably high accuracy.

Resolution. - The resolution for singly and doubly charged mercury ions is shown in figures 18(a), (b), and (c) as a function of a/q, inlet particle energy, and quadrupole rf voltage, respectively. Shown also in figure 18(a) is the theoretical resolution from equation (B12).

The experimental resolution was in accord with that predicted by theory at the design resolution of 10 (a/q = 0.310) and was essentially independent of inlet particle accelerating voltage. It should be emphasized that the resolutions obtained with singly and doubly charged mercury ions are similar. This would be expected for the selected mode of quadrupole mass filter operation, that is, variable frequency for a fixed voltage ratio. In this mode, all charged particles accelerated through a constant potential have the same degree of resolution, independent of their amu/z value. This is not necessarily the case for the variable voltage mode (ref. 2) and is one of the distinct advantages of the variable frequency mode.

As shown in figure 18(b), for the design a/q of 0.310 and a constant V of 1000 volts, the resolution agrees well with theory as the particle energy is increased from 2000 to 24 000 volts. Above 24 000 volts, the resolution dropped at a rate less than that predicted from theory, which indicates that the theory is perhaps conservative in predicting the maximum resolution obtainable.

In figure 18(c), for the design a/q of 0.310 with a particle accelerating voltage of 2000 volts, the experimental effect of varying the quadrupole rf voltage on resolution is compared with the design equations (B12) and (B15). Although a 10-percent deviation of the experimental data can be noted in figure 18(c), the overall effect of this deviation on the experimentally determined amu/z distribution would be negligible because a 10-percent variation in resolution about the design value results in a change of the amu/z distribution error ϵ_1 of 0.0002 (see appendix B for details).

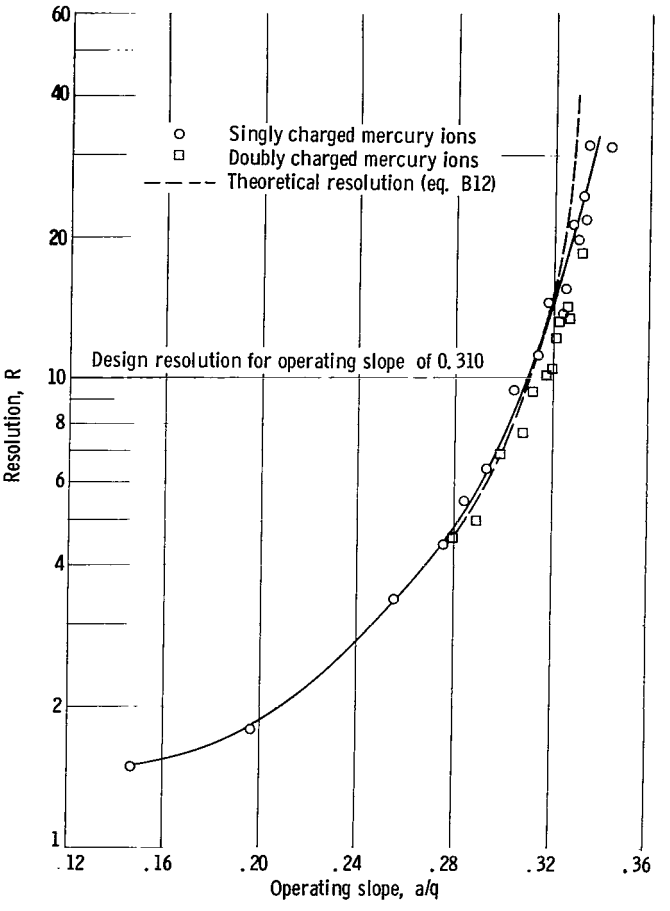

(a) Effect of operating slope. Net accelerating potential, 2000 volts; applied rf voltage, 1000 volts.

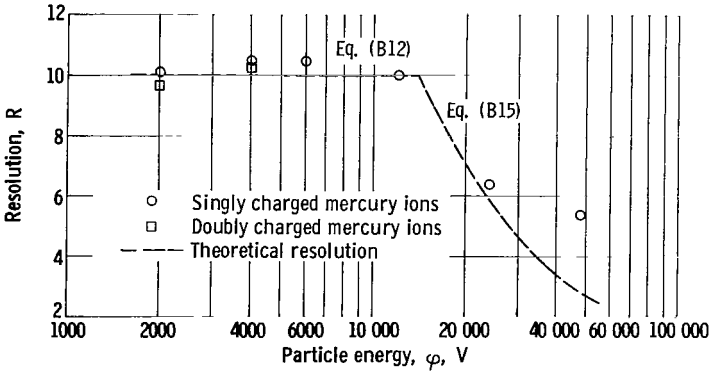

(b) Effect of particle energy. Operating slope, 0.310; applied rf voltage, 1000 volts.

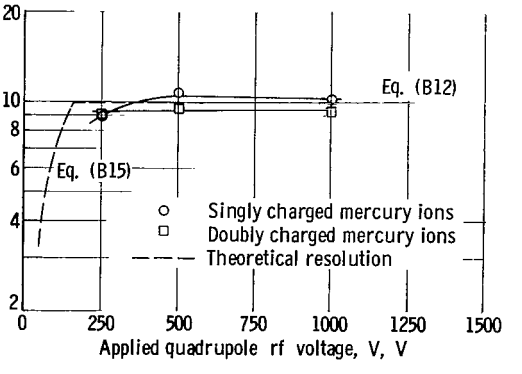

(c) Effect of rf voltage. Operating slope, 0.310; net accelerating potential, 2000 volts.

Figure 18. - Experimental resolution. Ion chamber potential, 110 volts; total thrustor beam current, 12×10^{-6} ampere.

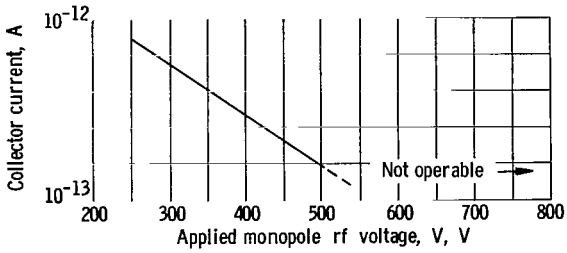

Figure 19. - Variation of collected current of singly charged mercury ions with rf voltage. Ion chamber potential, 110 volts; total thrustor beam current, 12×10^{-6} ampere; net accelerating potential, 2000 volts.

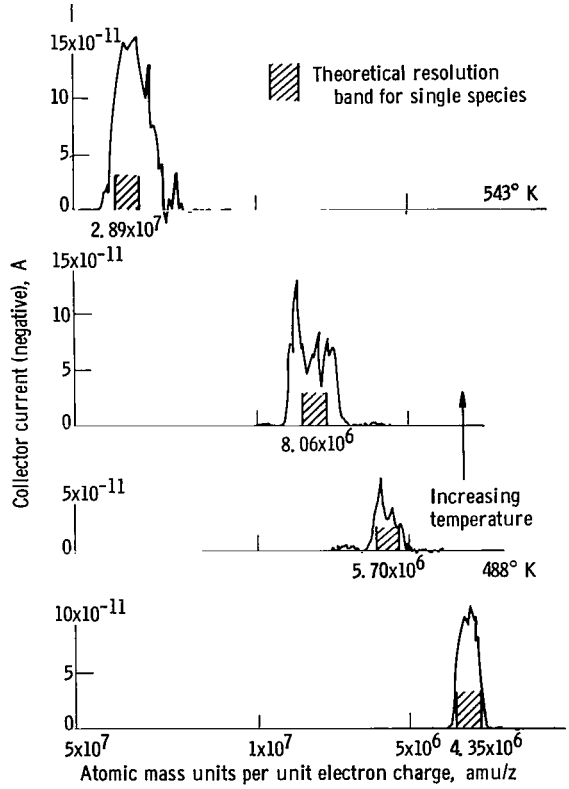

Figure 20. - Effect of increasing saturated vapor stagnation temperature from 488° to 543° K on particle distribution in continuum flow regime with mercurous chloride.

In summary, the experimental calibration has shown that the amu/z collected current intensity and resolution, as obtained with this quadrupole mass filter, are suitable for determining the $\langle$ amu/z$\rangle$ over a relatively wide range of inlet operating conditions.

Monopole mass spectrometer calibration. - The theory of operation of the monopole mass spectrometer is described in appendix B. Compared with the quadrupole, the monopole has several apparent advantages such as simplified construction and electronic design, (ref. 6); however, transmission, as noted in appendix B, should be theoretically reduced. The variation of collected current as a function of monopole rf voltage is presented in figure 19. It was not possible to obtain traces with the monopole at rf voltages greater than 500 volts. Qualitatively it would be expected that, with increasing rf voltage, the focusing effect of the monopole spectrometer would become stronger, and this in turn would result in a larger fraction of the particles striking the right-angled electrode. As shown in figure 19, the collected current was of the order of 10^{-13} to 10^{-12} ampere compared with 10^{-10} to 10^{-9} ampere for the quadrupole mass filter for equivalent thrustor operating conditions and equivalent entrance apertures; consequently, the monopole spectrometer appears to be relatively unsatisfactory for colloid-thrustor exhaust-beam analysis.

Colloid Application

Application of quadrupole to charged colloid beam. - Quadrupole traces of the colloid thrustor exhaust spectra with mercurous

chloride as the propellant are shown in figure 20 (from ref. 18) for a range of vaporizer temperatures corresponding to continuum flow in the colloid nozzle. Only the initial and final temperatures are shown in figure 20. Because the amount of propellant capacity was limited and the conditions corresponding to continuum flow entail relatively high flow rates, it was not possible to allow exact stepwise equilibrium temperature traces to be obtained.

In the continuum flow regimes, a high degree of supersaturation would be expected because of expansion in the nozzle. A high degree of supersaturation produces a rapid formation of nuclei by homogeneous condensation. These nuclei continue growth in the stream until they reach their ultimate size at the nozzle exhaust (refs. 15 and 19). As shown in figure 20, a high-intensity peak of charged colloids was observed. The theoretical resolution band for a single species is shown for comparison with the actual, observed trace. Although a particle growth model has not been satisfactorily established, by assuming thermodynamic equilibrium, and the classical liquid-drop theory of condensation to hold, a narrow distribution of colloid mass would be expected (ref. 18). The narrow particle size distribution obtained was characteristic of all data taken at conditions corresponding to continuum flow.

Comparison of colloid mass determination. - Comparisons were made of various colloid masses determined previously by photomicrographs and thrust-and-current measurements. The results are summarized in the following table:

Method of measurement	Indicated amu/z	Source	Temperature of vaporizer, ^{o}K
Photomicrographs	1.7 to 3.0×10^{6}	Ref. 14	488
Thrust and current	1.2 to 2.4×10^{6}	Ref. 15	488
Quadrupole	4.35×10^{6}	-------	488

A necessary assumption in this comparison is that the colloidal particles in the photomicrographs are singly charged. The amount and direction of difference in amu/z for the different methods indicate that the single charge assumption is reasonable.

The photomicrographs, previously reported in reference 14, were obtained with a close control of mass flow. Equilibrium conditions were attained in the vaporizer and a shutter was then opened momentarily to expose a silicon dioxide film to the colloid exhaust beam. The average particle masses determined from photomicrographs are in reasonable agreement with the quadrupole mass filter data; however, the photomicrographs indicated a distribution much wider than that indicated with the quadrupole mass filter. This is not surprising in view of the assumptions that were required to determine the distribution from the photomicrographs. For example, it was necessary to assume that no evaporation or agglomeration had occurred during the collection and examination,

and that the electron beam impinging on the colloid sample (during analysis) did not vaporize or affect apparent size.

Thrust measurements entail complexity in experimental procedure, as outlined in reference 15, that could introduce uncertainty in results. For example, it was necessary to assume that the particles were of uniform size and that the beam space charge did not exert an electrostatic force on the target.

The agreement of all the methods is considered to be remarkably good particularly when the accuracy of the various methods is considered. It is expected, however, that the quadrupole mass filter data are more reliable than either the photomicrographs or thrust-and-current measurements, since it samples discrete colloids in the beam. The amu/z distribution can be obtained directly from the quadrupole traces, and the error in measurements has been shown to be well within 7 percent.

Application of $\langle amu/z \rangle$ spectrum to thrustor performance. - The effect of measured amu/z distribution on thrustor efficiency is shown in the following table, where the distribution efficiency is determined from equation (C2). The values given are not to be confused with the overall efficiency as would be determined from equation (1). Due to a high neutral flow rate and limited voltage in the present thrustor, the overall efficiency was much too low to be useful for meaningful comparison with other electrostatic thrustors.

amu/z	Distribution efficiency, (eq. (C2))
4.35×10^{6}	0.999
5.70×10^{6}	1.000
8.06×10^{6}	.994
2.89×10^{7}	.993

Thus, in the best cases (which is also the region of most interest, i.e., smallest amu/z) a loss in efficiency of less than 0.1 percent was observed, which is probably representative of the 0.1 percent error permissible in the determination of the amu/z. At the higher amu/z values, where the loss in efficiency is as great as 0.7 percent, it is likely that some amu/z distribution has occurred (only 0.1 percent loss can be accounted for in ϵ_1 at a resolution of 10 (see appendix C).

CONCLUSIONS

As part of an overall program to determine the feasibility of colloid thrustors, a quadrupole mass filter was designed, calibrated, and used to analyze a beam produced

by such a thrustor. The performance of this mass filter was in good agreement with design criteria, and its value for thrustor evaluation was demonstrated.

It was verified that (1) the distribution efficiency can be measured within an error of 0.1 percent at the design resolution of 10; (2) the atomic mass units per unit electron charge can be measured within about 2.5 percent at the design resolution of 10; (3) the quadrupole measured the relative abundance of known species within an accuracy of 3 percent; (4) the resolution was substantially independent of the atomic mass units per unit electron charge.

A region of quadrupole operation, where the collected current was insensitive to operating slope, could not be established when the particle inlet velocity corresponded to more than the radiofrequency voltage; however, the inherent operating-slope variation (due to impressed voltages) over the atomic mass units per unit electron charge sweep could be controlled to allow a maximum variation of 3 percent in the collected current.

A maximum entrance aperture (i.e., aperture = quadrupole field radius) was most desirable for colloid-thrustor evaluation. Also, the loss in overall efficiency due to the beam spectra was determined to be well within 7 percent, the selected quadrupole design limit of error. The quadrupole mass filter gave more accurate information concerning the exhaust spectra of a colloid thrustor than photomicrographs or thrust-and-current measurements.

Finally, it was demonstrated that a quadrupole mass filter can be satisfactorily modified to operate in the variable frequency mode over the full range of atomic mass units per unit electron charge spectra anticipated in colloid-thrustor application.

Lewis Research Center,
National Aeronautics and Space Administration,
Cleveland, Ohio, June 15, 1965.

APPENDIX A

SYMBOLS

a	parameter defined in eq. (B6a)
amu/z	atomic mass units per unit electron charge
Δamu/z	amu/z band width
$\langle$amu/z$\rangle$	average amu/z as determined from amu/z spectrum
c	speed of light, 2.9979×10^{8} m/sec
D	inlet aperture diameter, m
e	electron charge, 1.6×10^{-19} C
$\vec{F}$	total force on charged particle
f	frequency of applied rf field, cps
J_B	total thrustor beam current, A
j*(amu/z)	distribution function of amu/z obtained by normalizing collector current variation with amu/z to unity
k	constant
L	length of quadrupole mass filter, m
ℓ	quadrupole inlet aperture length
m	ion or colloid mass, kg
$\dot{m}_c$	charged particle mass flow, kg/sec
$\dot{m}_T$	total mass flow, kg/sec
n	number of cycles spent in quadrupole, defined in eq. (B13)
P_ℓ	total power loss, W
q	parameter defined in eq. (B7a)
R	resolution
r	radius of quadrupole rods, m
$\vec{r}$	position vector
r_a	radius of quadrupole inlet aperture, m
r_o	radius of quadrupole focusing field, m
t	time, sec
U	applied d-c voltage, V
V	applied rf voltage, V
V_L	applied voltage at sending end on quadrupole rod, V
V_o	receiving end voltage on quadrupole rod, V
x, y	coordinates normal to quadrupole axis, m
Z	axial distance, m

z	number of electrons e per ion or colloidal particle
α	difficulty factor defined in eq. (2)
β	factor due to variation in collected current intensity
ϵ	overall error in determining thrustor efficiency
ϵ_1	distribution error as determined by eq. (C5)
ϵ_2	amu/z error as determined by eq. (C8)
ϵ_3	rf quadrupole voltage error, $\Delta V/V$
ϵ_4	radius of quadropole focusing field error, $\Delta r_o/r$
ϵ_5	frequency error, $\Delta f/f$
ϵ_6	error due to variation in collected current intensity
η	overall thrustor efficiency defined in eq. (1)
η_d	distribution efficiency defined in eq. (C2)
η_p	power efficiency defined in eq. (C1a)
η_t	power efficiency including effects of distribution, defined in eq. (C1b)
η_u	utilization efficiency defined in eq. (C3)
λ	wavelength of applied rf signal
ξ	time variable, $\omega t/2$
Φ	potential of focusing field, V
Φ_o	form of applied voltages, V
φ	net accelerating potential also equivalent to particle energy, V
Ω	step function
ω	angular frequency of applied electric field, rad/sec

Subscripts:

1	Intersection with line B on stability diagram (fig. 21)
2	Intersection with line A on stability diagram (fig. 21)

APPENDIX B

SUMMARY OF BASIC QUADRUPOLE MASS FILTER THEORY

Quadrupole Mass Filter

The theory of quadrupole operation and basic design equations has been presented by Paul, et al. (ref. 2). Pertinent theory and operation will be summarized for convenience. The quadrupole mass filter, shown schematically in figure 1(a) (p. 3), consists of four cylindrical rods, equally spaced, about a tangent circle of radius r_o. The rf voltages $\pm V \cos \omega t$ and d-c voltages U are applied as shown. Ideally, if hyperbolic rods are used as the field-forming electrodes, the potential distribution within the quadrupole is given by

$$\Phi = (U + V \cos \omega t) \frac{x^2 - y^2}{r_o^2} \tag{B1}$$

However, cylindrical rods with a radius about 1.15 times the tangent circle radius are used as the field-forming electrodes because they are simpler to fabricate. It has been shown that this configuration can produce the hyperbolic field to within ±1 percent (ref. 20).

The electrical force $\vec{F}$ on a charged particle is given by $\vec{F} = -e\nabla\Phi \equiv \vec{ma}$. Substituting Φ from equation (B1) yields

$$m\ddot{x} + 2ze(U + V \cos \omega t) \frac{x}{r_o^2} = 0 \tag{B2}$$

$$m\ddot{y} - 2ze(U + V \cos \omega t) \frac{y}{r_o^2} = 0 \tag{B3}$$

$$m\ddot{z} = 0 \tag{B4}$$

In order that equations (B2) and (B3) be in a more tractable form, the following change of variables is made (ref. 2):

$$2\xi = \omega t \tag{B5}$$

$$a = \frac{8zeU}{mr_o^2\omega^2} \tag{B6a}$$

$$q = \frac{4zeV}{mr_o^2\omega^2} \tag{B7a}$$

Carrying out this change of variables results in

$$\frac{d^2x}{d\xi^2} + (a + 2q \cos 2\xi)x + 0 \tag{B8}$$

$$\frac{d^2y}{d\xi^2} - (a + 2q \cos 2\xi)y = 0 \tag{B9}$$

Equations (B8) and (B9) are in the form of the Mathieu equations whose general solutions are known (ref. 21).

The solution of the Mathieu equations, as applied to the operation of a quadrupole

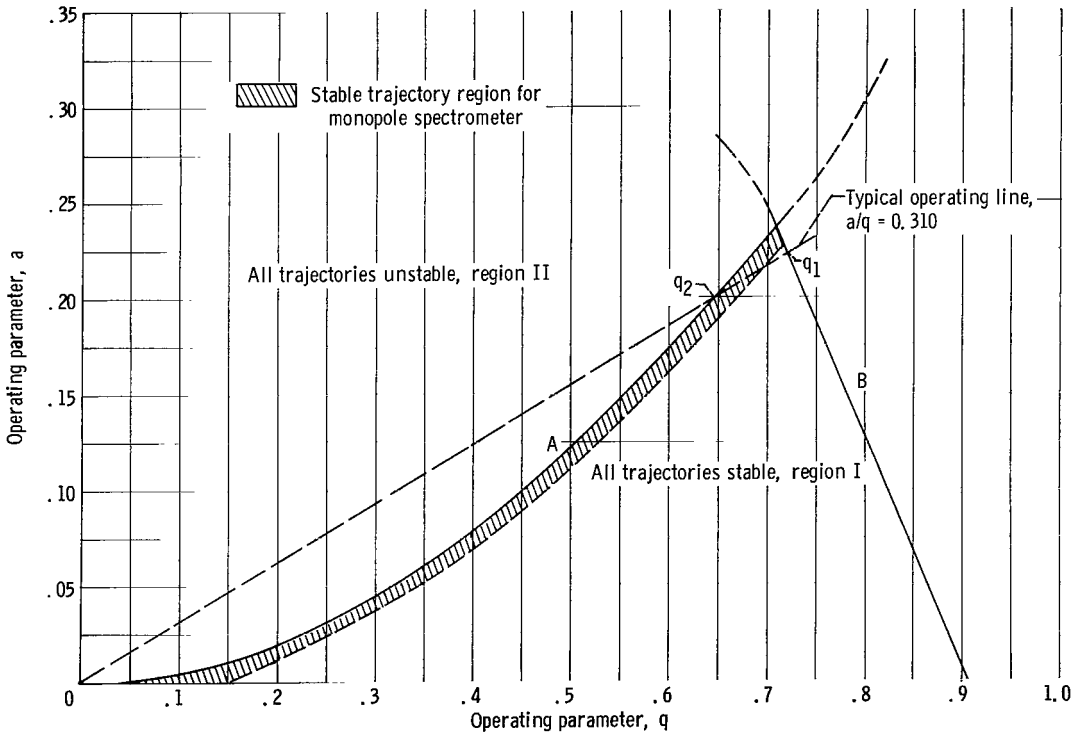

Figure 21. - Stability diagram for quadrupole mass filter operation.

mass filter, is plotted in figure 21. The solution is characterized by a stable region (I) where the amplitude of oscillation (x and y) remains bounded and an unstable region (II) where the amplitude of oscillation is exponentially divergent. Equations (B6a) and (B7a) are used to relate the quadrupole operating parameters (U, V, r_o, $f = \omega/2\pi$) to an operating point a, q on the stability plot (fig. 21). Any operating point in the area under curve B on the a/q plot (fig. 21) represents conditions for a stable solution in the x-direction, while a point falling in the area under curve A represents a condition for a stable solution in the y-direction. Therefore, a condition necessary to obtain a stable trajectory is that the operating point falls within the area under curves A and B. The ratio m/e will be expressed as an equivalent amu/z (as used in ref. 1) for this report. Equations (B6a) and (B7a) can be arranged as

$$a = \frac{7.664\times10^{8}\ U}{(amu/z)r_o^2\omega^2} \tag{B6b}$$

$$q = \frac{3.832\times10^{8}\ V}{(amu/z)r_o^2\omega^2} \tag{B7b}$$

Therefore, for fixed values of the quadrupole parameters all particles of the same amu/z have the same operating point, that is, the same values of a and q. Since the ratio of a to q is independent of amu/z, any straight line passing through the origin of the stability plot contains operating points for all values of amu/z (see fig. 21). The particular line used with slope 2U/V is referred to as the operating line. The only particles with a stable trajectory are those whose operating points lie along the segment of the operating line between q_1 and q_2 in figure 21. Of these particles, only a constant fraction are capable of reaching the collector because stable particles near the outer perimeter of the tangent circle can impinge on the quadrupole rods (amplitude of oscillation greater than the initial distance of the particles to the quadrupole rods). The transmission of the quadrupole for a given amu/z will therefore be defined as the ratio of the current reaching the collector for a given a/q setting to the current arriving at the inlet aperture for the same amu/z.

There are two methods of scanning operating points along the operating line at a constant ratio of a/q (ref. 2). The first method requires holding the frequency of excitation constant while varying the voltages; the second method requires holding the voltages constant while varying the frequency of excitation. It will be shown that the variable frequency method is more applicable to colloid beam analysis; hence this method will be used to discuss quantitatively the quadrupole operational characteristics. The stability

plot and equation (B7b) can be used to show that a particle of given amu/z will have a stable trajectory over a frequency band given by

$$\Delta f = \frac{3.12\times10^3\ V^{1/2}}{r_o(amu/z)^{1/2}\ (q_2 - q_1)^{1/2}} \tag{B10}$$

The magnitude of $q_2 - q_1$ depends only on the slope of the operating line 2U/V.

A more direct interpretation of the quadrupole operation is possible if the frequency corresponding to each point is converted to an equivalent amu/z by setting $q = 0.706$ in equation (B7b). This is the value of q associated with infinite resolution (i. e., the maximum stable point on the stability diagram (fig. 21)).

The quadrupole transmits a particular amu/z species over a finite amu/z band. The band width Δamu/z can be obtained by noting, from equation (B7b), that amu/z is proportional to 1/q, or, amu/z = k(1/q). Writing this expression for q_1, q_2, and $q_{0.706}$ (see fig. 21) and combining them gives the following expression for the amu/z band width:

$$\Delta amu/z = \frac{q_1 - q_2}{q_1 - q_2}\, q_{0.706}(amu/z) \tag{B11a}$$

The theoretical resolution can now be defined from equation (B11a) as the ratio of the amu/z divided by the amu/z band or,

$$R_{theor} = \frac{amu/z}{\Delta amu/z} = \frac{q_1 q_2}{(q_1 - q_2)q_{0.706}} \tag{B11b}$$

The resolution can also be expressed in terms of the quadrupole operating parameters U and V as

$$R \approx \frac{0.126}{0.16784 - \frac{U}{V}} \tag{B12}$$

This expression results from an approximation to the solution of the Mathieu equations (ref. 22). Clearly, the maximum ratio of U/V for stable trajectories is 0.16784.

From equation (B12) it is apparent that, as the operating slope increases, the transmitted amu/z band decreases because the number of particles with unstable trajectories

increases. However, this effect takes place only if the particles with unstable trajectories are removed from the field before they can reach the collector. This removal occurs only if they remain in the quadrupole field for a certain minimum number of rf voltage cycles so that their amplitude becomes sufficiently large. If all particles remain in the quadrupole field less than the minimum number of required cycles, the resolution would not increase with an increase in a/q.

It has been shown (ref. 2) that the minimum number of cycles to remove unstable particles is approximately equal to

$$n \approx 3.5 \sqrt{R} \tag{B13}$$

This number can be used to obtain an expression for maximum theoretical resolution by noting that the frequency of oscillation for a particle initially accelerated through a potential φ, that undergoes n cycles in a quadrupole of length L is

$$f = \frac{n \sqrt{2(e/m)\varphi}}{L} \tag{B14}$$

Substituting equation (B13) into equation (B14) and equating this oscillation frequency to the operating frequency determined from equation (B7b) result in the following expression for maximum theoretical resolution:

$$R \approx \frac{5.86 \times 10^{-3} L^2 V}{r_o^2 \varphi} \tag{B15}$$

Two equations are now available for the resolution. Equation (B12) does not take into account the inlet particle velocity (which affects the number of cycles required to remove unstable trajectories), and equation (B15) does not take into account the operating slope 2U/V required for a given resolution. Consequently, in order to determine the applicable theoretical resolution, both equations (B12) and (B15) must be evaluated, and the one that indicates the lowest resolution is the controlling equation.

It is apparent from equation (B15) that, if all particles are accelerated through a constant potential φ for a given quadrupole configuration, the resolution will be directly proportional to the rf voltage V. If operation is then such that equation (B12) equals equation (B15), all particles will be resolved to the same degree, and it would be expected that the transmission of each species will be the same. For the investigation herein, the variable-frequency mode of operation was used to satisfy this condition. In this mode of operation, the rf voltage V is fixed, the d-c voltage U is fixed, and

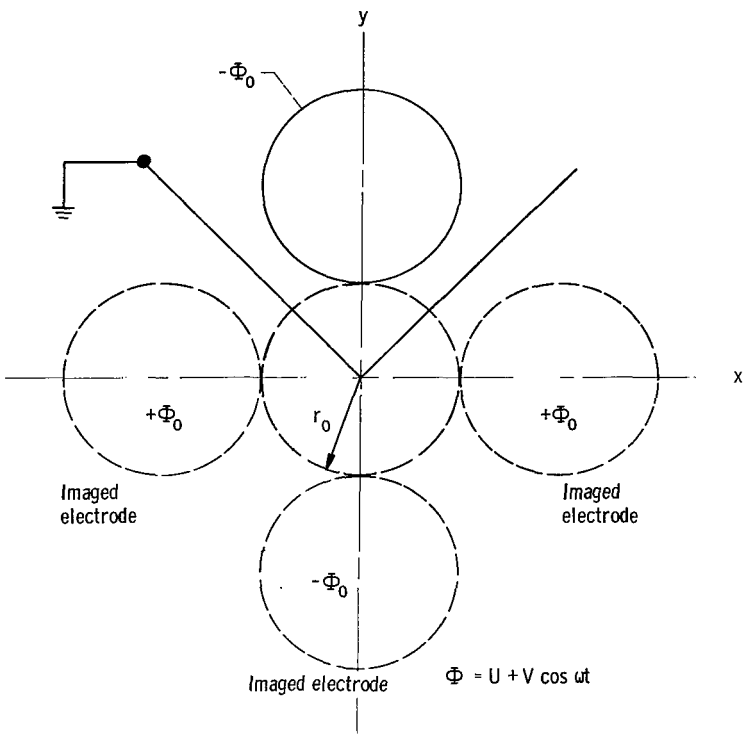

Figure 22. - Schematic drawing of cross section of monopole mass spectrometer.

the frequency of excitation is varied to examine the required range of amu/z distribution. It should be noted that, for the alternate mode of operation (fixed frequency and variable voltage), an impractical range of voltages would be required to obtain the same fixed resolution and constant transmission.

Monopole Mass Spectrometer

A cross section of the monopole mass spectrometer is shown schematically in figure 22. The filtering field is established by only two electrodes (the cylindrical rod and a right-angled ground electrode). Operation of the monopole spectrometer is somewhat similar to that of the quadrupole; however, the stability region is represented by the crosshatched narrow band parallel to the A line of figure 21 (p. 32). It is apparent from figure 21 that, for any a/q operating slope up to the peak of the a/q stability diagram, the crosshatched band width (indicative of resolution) will remain approximately constant. Consequently, a major theoretical advantage of the monopole spectrometer is that the ratio of the d-c and rf voltage may vary during a trace without appreciably affecting resolution or transmission. As a result, the electronic circuitry and particularly the voltage control can be greatly simplified. These advantages are offset by impingement of the particles on the right-angled ground electrode and by the reduced

inlet aperture (one quarter of a circle). This combination reduces the maximum current that can reach the collector. For the application herein, this reduction in collected current intensity could (and in fact did) negate the advantages afforded by the simplification of electron circuitry.

APPENDIX C

ERROR DETERMINATIONS FOR COLLOID APPLICATION OF QUADRUPOLE DESIGN

As shown in reference 1, the thrustor efficiency is a function of the amu/z spectrum. It is thus required that this spectrum be known accurately in order to determine thrustor efficiencies. Thrustor power efficiency is defined as the ratio of the actual jet output power to the input power to the thrustor. In the case of paraxial flow electrostatic thrustors, this efficiency is expressed as

$$\eta_p = \frac{1}{1 + \frac{P_\ell}{J_B \varphi}} \tag{C1a}$$

where P_ℓ is total power loss, J_B is beam current, and φ is the net accelerating potential. As discussed in reference 1, the power efficiency for the nonideal electrostatic thrustor must include loss effects that arise not only because of nonparaxial flow, but also because of possible distribution in particle mass-to-charge ratios. This distribution effect is of major concern with regard to the colloid thrustor and when accounted for results in the following expression

$$\eta_t = \frac{1}{1 + \frac{P_\ell}{J_B \varphi}} \eta_d \tag{C1b}$$

where

$$\eta_d = \frac{\left[\int_0^\infty (\text{amu}/z)^{1/2} \, j^*(\text{amu}/z) d(\text{amu}/z)\right]^2}{\int_0^\infty (\text{amu}/z) j^*(\text{amu}/z) d(\text{amu}/z)} \tag{C2}$$

and $j^*(\text{amu}/z)$ is the distribution function of amu/z, which is obtained by normalizing the variation in collector current with amu/z to unity. In addition, the utilization efficiency η_u is defined as

$$\eta_u \equiv \frac{\dot{m}_c}{\dot{m}_T} = \frac{10.43\times10^{-8}\, J_B\langle amu/z\rangle}{\dot{m}_T} \tag{C3}$$

where $\dot{m}_T$ is the total mass flow, $\dot{m}_c$ is the charged particle mass flow, and $\langle amu/z\rangle$ is the average value determined from the spectrum.

Combining equations (C1b), (C2), and (C3) results in the following expression for overall thrustor efficiency:

$$\eta = \frac{1.043\times10^{-8}\, J_B}{\dot{m}_T\left(1 + \frac{P_\ell}{J_B\varphi}\right)}\, \eta_d \langle amu/z\rangle \tag{C4}$$

Examination of equation (C4) indicates that determination of the overall colloid thrustor efficiency η requires a knowledge of the amu/z spectrum obtained from the quadrupole data as well as the total beam current, power losses, total mass flow, and net accelerating potential of the thrustor.

Consideration of the probable errors in the experimental determination of $\eta_d \langle amu/z\rangle$ indicated that a value of 7 percent might be reasonable. This 7-percent error was considered the allowable error in designing the quadrupole system and can be expressed in terms of quadrupole parameters V, r_o, f, and resolution R.

Equation (C2), the expression for η_d, can be expressed as a function of resolution only. For simplicity in evaluation, a rectangular distribution of collected current variation with amu/z is assumed, which results in a normalized amu/z distribution function of the form

$$j^*(amu/z) = \frac{\Omega\left[(amu/z) - (amu/z)_1\right] - \Omega\left[(amu/z) - (amu/z)_2\right]}{\Delta amu/z}$$

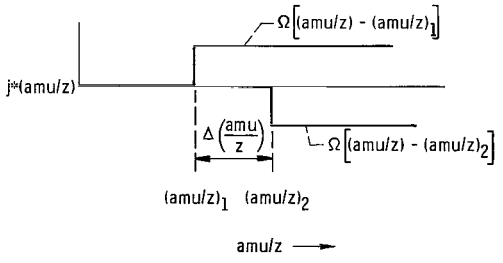

In this equation Ω quantities are step functions of the form depicted in the sketch. Performing the integration indicated in equation (C2) with this substitution and then expressing $amu/z = [(amu/z)_1 + (amu/z)_2]/2$ and $\Delta amu/z = (amu/z)/R$ result in

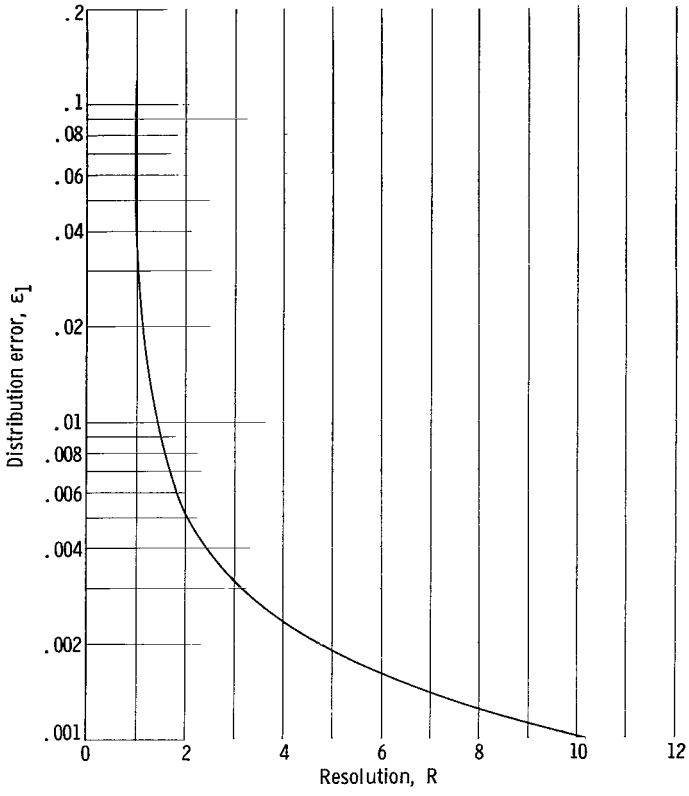

Figure 23. - Effect of resolution on distribution error (rectangular amu/z distribution).

$$\epsilon_1 = 1 - \frac{4}{9}\left\{\frac{\left[(2R+1)^{3/2} - (2R-1)^{3/2}\right]^2}{(2R+1)^2 - (2R-1)^2}\right\} \tag{C5}$$

where ϵ_1 is the error $\Delta\eta_d/\eta_d$ due to the finite band width (resolution) of a single amu/z species and will hereinafter be referred to as the distribution error. Equation (C5) is plotted in figure 23. For a design resolution of 10, $\epsilon_1 = 0.001$. It is apparent that a large error could be incorporated into the determination of η_d when the resolution is low.

The accuracy in determining $\langle \text{amu/z} \rangle$ is dependent on the accuracy of determining the measured distribution. The errors involved in determining this distribution come from measuring the values of voltage, field radius, and frequency. From equation (B7b),

$$\text{amu/z} = \frac{kV\beta}{r_o^2 f^2}$$

where β is a factor added here to account for possible variations in collected current during a frequency scan.

The maximum change in amu/z can therefore be written as

$$\Delta\text{amu/z} = \text{amu/z} - \frac{k(V - \Delta V)(\beta - \Delta\beta)}{(r_o + \Delta r_o)^2 (f + \Delta f)^2} \tag{C6}$$

Normalizing the variables in equation (C6) results in the following expression:

$$1 - \frac{\Delta amu/z}{amu/z} = \frac{\left(1 - \frac{\Delta V}{V}\right)\left(1 - \frac{\Delta \beta}{\beta}\right)}{\left(1 + \frac{\Delta r_o}{r_o}\right)^2 \left(1 + \frac{\Delta f}{f}\right)^2} \tag{C7}$$

Defining ϵ_2, ϵ_3, ϵ_4, ϵ_5, and ϵ_6 as $\frac{\Delta amu/z}{amu/z}$, $\frac{\Delta V}{V}$, $\frac{\Delta r_o}{r_o}$, $\frac{\Delta f}{f}$, and $\frac{\Delta \beta}{\beta}$, respectively, gives equation (C7) in the form

$$\epsilon_2 \approx 1 - \frac{(1 - \epsilon_3)(1 - \epsilon_6)}{(1 + \epsilon_4)^2 (1 + \epsilon_5)^2} \tag{C8}$$

The error in the term $\eta_d \langle amu/z \rangle$, which is the quadrupole contribution to the error in determining the overall thrustor efficiency, can be expressed as

$$\epsilon = 1 - \left[(1 - \epsilon_1)(1 - \epsilon_2)\right] \tag{C9}$$

where the terms $1 - \epsilon_1$ and $1 - \epsilon_2$ represent the contribution from equations (C5) and (C8), respectively. Of the terms in equation (C8), error values were assigned as follows:

(1) ϵ_1, 0.1 percent, error due to imperfect resolution (eq. (C5))

(2) ϵ_3, 1 percent, error in rf voltmeter reading

(3) ϵ_4, 1.5 percent estimated error in field simulation

(4) ϵ_5, 0.5 percent, error in recording the frequency

(5) ϵ_6, 2 percent estimated error due to variation in collected current intensity

When substituted into equation (C9), the preceding values yield the assumed total error in quadrupole measurements of 7 percent.

REFERENCES

1. Mickelsen, William R.; and Kaufman, Harold R.: Status of Electrostatic Thrustors for Space Propulsion. NASA TN D-2172, 1964.

2. Paul, W.; Reinhard, H. P.; and von Zahn, U.: The Electric Mass Filter as a Mass Spectrometer and Isotope Separator. Trans. No. TR-3484, AEC, 1958.

3. Mosharrafa, M.; and Oskam, H. J.: Design and Construction of a Mass-Spectrometer for the Study of Basic Processes in Plasma Physcis, Tech. Rept. No. 2 (NP-11459), July 1960-July 1961, AEC, 1961.

4. Woodward, C. E.; and Crawford, C. K.: Development of a Quadrupole Mass Spectrometer. Tech. Rept. No. 194 (AFML-TR-64-400), M.I.T., Dec. 1964.

5. Brubaker, Wilson M.; and Tuul, Johannes: Performance Studies of a Quadrupole Mass Filter. Rev. Sci. Instr., vol. 35, no. 8, Aug. 1964, pp. 1007-1010.

6. von Zahn, Ulf: Monopole Spectrometer, A New Electric Field Mass Spectrometer. Rev. Sci. Instr., vol. 34, no. 1, Jan. 1963, pp. 1-4.

7. Krohn, Victor E., Jr.: Glycerol Droplets for Electrostatic Propulsion. Vol. 9 of Prog. in Astronautics and Aeronautics, E. Stuhlinger, ed., Academic Press, Inc., 1963, pp. 435-440.

8. Cohen, E.: Research on the Electrostatic Generation and Acceleration of Submicron-Size Particles. Rept. No. ARL-63-88, Space Technology Lab., Inc., May 1963.

9. Cox, A. Lucille: Condenstaion Colloid Ion Source. Rept. No. ASD-TDR-63-825, Ion Physics Corp., June 12, 1964.

10. Gignoux, D.; Anton, H. F.; and Shea, J. J.: Development of a Charged Colloid Source for Electrostatic Propulsion. NASA CR 54176, 1964.

11. Ryder, John D.: Networks, Lines, and Fields. Second ed., Prentice-Hall, Inc., 1955, ch. VI.

12. Chupp, Warren W.; and Heard, Harry G.: Spark Damage and High Voltage Breakdown of Metals in Vacuum at 14 Megacycles. Rept. No. UCRL-1962 (Rev.), Univ. Calif., 1954.

13. Reader, Paul D.: Investigation of a 10-Centimeter-Diameter Electron-Bombardment Ion Rocket. NASA TN D-1163, 1962.

14. Norgren, Carl T.: Onboard Colloidal Particle Generator for Electrostatic Engines. Vol. 9 of Prog. in Astronautics and Aeronautics, E. Stuhlinger, ed., Academic Press, Inc., 1963, pp. 407-434.

15. Goldin, Daniel S.; and Norgren, Carl T.: Thrust Measurements of Colloidal Particles as an Indication of Particle Size and Thrustor Operation. Paper No. 63050-63, AIAA, 1963.

16. Pawlik, Eugene V.; Margosian, Paul M.: and Staggs, John F.: A Technique for Obtaining Plasma-Sheath Configurations and Ion Optics for an Electron-Bombardment Ion Thrustor. NASA TN D-2804, 1965.

17. Brode, Robert B.: The Quantitative Study of the Collisions of Electrons with Atoms. Rev. Mod. Phys., vol. 5, Oct. 1933, pp. 257-279.

18. Norgren, Carl T.; and Goldin, Daniel S.: Experimental Analysis of the Exhaust Beam from a Colloid Thrustor. Paper No. 64-674, AIAA, 1964.

19. Griffin, James L.: Digital Computer Analysis of Condensation in Highly Expanded Flows. Rept. No. ARL 63-206, Univ. Michigan, Nov. 1963.

20. Dayton, I. E.; Shoemaker, F. C.; and Mozley, R. F.: The Measurement of Two-Dimensional Fields. Pt. II: Study of a Quadrupole Magnet. Rev. Sci. Instr., vol. 25, no. 5, May 1954, pp. 485-489.

21. McLachlan, N. W.: Theory and Application of Mathieu Functions. Clarendon Press (Oxford), 1947.

22. Paul, W.; und Raether, M.: Das elektrische Massenfilter. Z. Physik, bd. 140, 1955, pp. 262-273.

"The aeronautical and space activities of the United States shall be conducted so as to contribute . . . to the expansion of human knowledge of phenomena in the atmosphere and space. The Administration shall provide for the widest practicable and appropriate dissemination of information concerning its activities and the results thereof."

—NATIONAL AERONAUTICS AND SPACE ACT OF 1958

NASA SCIENTIFIC AND TECHNICAL PUBLICATIONS

TECHNICAL REPORTS: Scientific and technical information considered important, complete, and a lasting contribution to existing knowledge.

TECHNICAL NOTES: Information less broad in scope but nevertheless of importance as a contribution to existing knowledge.

TECHNICAL MEMORANDUMS: Information receiving limited distribution because of preliminary data, security classification, or other reasons.

CONTRACTOR REPORTS: Technical information generated in connection with a NASA contract or grant and released under NASA auspices.

TECHNICAL TRANSLATIONS: Information published in a foreign language considered to merit NASA distribution in English.

TECHNICAL REPRINTS: Information derived from NASA activities and initially published in the form of journal articles.

SPECIAL PUBLICATIONS: Information derived from or of value to NASA activities but not necessarily reporting the results of individual NASA-programmed scientific efforts. Publications include conference proceedings, monographs, data compilations, handbooks, sourcebooks, and special bibliographies.

Details on the availability of these publications may be obtained from:

SCIENTIFIC AND TECHNICAL INFORMATION DIVISION

NATIONAL AERONAUTICS AND SPACE ADMINISTRATION

Washington, D.C. 20546